Marine Technology, Vol. 19, No. 1, Jan. 1982, pp. 1–22

3

Marine
Technology

Low-Frequency Dynamics of Moored Vessels

B. W. Oppenheim[1] and **P. A. Wilson**[2]

Three complete theories of the low-frequency dynamics of ships and disks moored with multileg mooring systems in deep water are derived, evaluated, and computerized. One theory is nonlinear; it includes the effects of cubic damping, nonlinear mooring forces and the excitation-yaw motion feedback, and it is handled by simulation. It yields random, regular and transient records, probabilities and statistics, exact and linearized transfer functions, and spectra of responses. The second theory is linear, solved in the frequency domain. The third is a static theory, which is a by-product of the linear one. Mooring lines of arbitrary compositions are considered.

1. Introduction

THIS PAPER presents several theoretical methods for predicting the low-frequency dynamics of large ships and disks moored in deep waters with multileg mooring systems.

The motions of moored vessels caused by the random environments have a very distinct spectral content. There are large and narrow peaks at low frequencies and smaller but wide peaks at high frequencies and the two regions have almost no overlap. There is also a large steady displacement. The terms "high" and "low" are used relative to the frequencies of the waves. The high-frequency motions have wave frequencies typically from 0.2 to 2 radians per second (rad/s). The low frequencies occur in the range from 0 to approximately 0.2 rad/s. The high-frequency motions are caused by the high-frequency hydrodynamic force associated with individual waves. This force has a zero mean and the motions caused by it are approximately linear with respect to wave amplitude and thus also of zero mean. The second-order hydrodynamic force (commonly called drift force) is proportional to the square of the wave amplitude and it has a mean level. This force is associated with occurrence of wave groups, with interactions between the high-frequency vessel motions and the high-frequency excitation, and with wave diffraction. The "direct current" (dc) component of the low-frequency force, together with the almost-steady wind and current forces, causes the static displacement of the moored vessel. The low-frequency part of the force causes slow oscillatory motions, since a moored vessel constitutes a mass-spring-damper oscillator. The damping and spring are typically small; consequently large resonant motions occur, larger in fact than the high-frequency ones.

The high-frequency dynamics are almost independent of water depth, except in the extremely shallow depths which are of no practical interest, and the magnitudes of the dynamic responses are proportional to the wave amplitude. The magnitudes of the low-frequency responses are approximately proportional to the depth. Therefore, the low-frequency theories alone can be regarded as asymptotic solutions of the total problem in deep waters. However, procedures for combining the low- and high-frequency parameters are available in [1].[3] The deepwater assumption is also introduced for simplifying the mathematical models. The low-frequency excitation is small; it causes large horizontal vessel motions because the horizontal damping and restoring forces are also small. On the other hand, the vertical damping and restoring forces are large on the types of vessels studied here; therefore the vertical low-frequency motions are small. The changes of state caused by the vertical motions can therefore be neglected if the water is deep, and this is the approach adopted herein.

The mooring systems considered are of the spread multileg type, sketched in Fig. 1. This type has evolved in offshore oil industry to be the most popular. It offers high positioning precision, flexibility, and reliability, as well as a quick deployment and easy maintenance. It has been routinely applied in water depths of up to approximately 1 km (3280 ft), using wire and chain mooring lines. The heavy weight of such lines precluded moorings in deeper waters. However, due to the recent advances in the technology of light synthetic ropes, this type can be expected to be extended to much deeper waters. The mathematical model derived is valid for an arbitrary composition of the mooring lines.

There are several inherent nonlinearities present in the system. The mooring forces are well known to be nonlinear and these introduce both nonlinear restoring forces and a nonlinear coupling in the equations of motion. The low-frequency oscillatory damping is viscosity-controlled and it is cubic in velocities. The low-frequency wave forces are quadratic in wave amplitude. These nonlinearities occur regardless of vessel type. If the vessel lacks circular symmetry, the environmental forces will also depend on the angles of incidence of the weather elements, that is, indirectly, on the vessel angular orientation in space. This constitutes a nonlinear feedback between the yaw motion and the excitation. Another nonlinearity arising from the angular orientation is the necessity of using two frames of reference for defining the terms in the equations of motion: the body frame, which moves with the vessel and in which the body forces are determined, and an earth frame, in which the mooring forces are defined, since the anchors are obviously attached to the earth. Thus, axis transformations must take place at each new state of

[1] B. W. Oppenheim, Ph.D. & Associates, Inc., Los Angeles, California.
[2] Ship Science, Southampton University, Southampton, England.
Presented at the September 11, 1980 meeting of the Los Angeles Metropolitan Section of THE SOCIETY OF NAVAL ARCHITECTS AND MARINE ENGINEERS.

[3] Numbers in brackets designate References at end of paper.

0025-3316/82/1901-0001$00.69/0

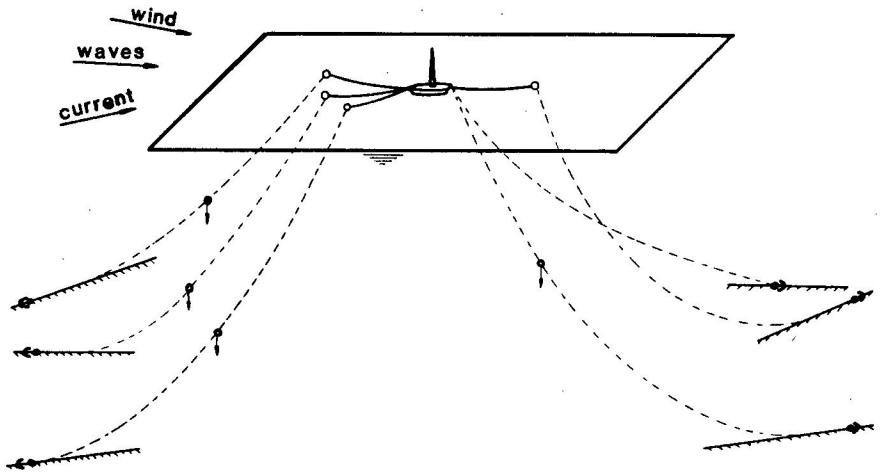

Fig. 1 Schematic configuration of multileg mooring

Nomenclature

$[a_{ij}]$ = 3*3 added-mass matrix
A = wave amplitude
A_{x_k}, A_{y_k} = kth fairlead coordinates in body frame
$[b_{ij}]$ = 3*3 matrix of linear damping coefficients
B = ship beam
BF = body frame
$B_{x_{Gk}}, B_{y_{Gk}}, B_{z_{Gk}}$ = kth anchor coordinates in global frame
$B_{x_{ok}}, B_{y_{ok}}, B_{z_{ok}}$ = kth anchor coordinates in natural equilibrium frame
$[c_{ij}]$ = 3*4 matrix of nonlinear damping coefficients
$[d_{ij}]$ = 3*3 matrix of linear mooring force coefficients, linearized at EF
D = water depth
D_x, D_y, D_ψ = surge, sway, and yaw components of damping force in body frame
E = total excitation force
E_x, E_y, E_ψ = components of E in body frame
$E_{x_E}, E_{y_E}, E_{\psi_E}$ = components of E in equilibrium frame
$E_{x_o}, E_{y_o}, E_{\psi_o}$ = components of E in natural equilibrium frame
$\bar{E}, \bar{E}_\psi$ = mean drift force and moment
E_E = relative oscillatory excitation force in equilibrium frame
EF = equilibrium frame
F_c = current force
$F_{c_x}, F_{c_y}, F_{c_\psi}$ = components of F_c in body frame
$F_{c_{x_o}}, F_{c_{y_o}}, F_{c\psi_o}$ = components of F_c in natural equilibrium frame
F_w = wind force
$F_{w_x}, F_{w_y}, F_{w_\psi}$ = components of F_w in body frame
$F_{w_{x_o}}, F_{w_{y_o}}, F_{w\psi_o}$ = components of F_w in natural equilibrium frame
g = gravitational acceleration
G_F, G_M = one-sided spectra of wave drift force and moment
G_F^0, G_M^0 = one-sided white spectra of wave drift force and moment
GF = global frame
G_w = one-sided wave spectrum
G_{EE} = one-sided measured spectrum of total excitation force
G_{xx} = one-sided measured spectrum of some response x
H = horizontal tension in mooring line
$H_F, H_{F_x}, H_{F_y}, H_M$ = transfer functions of total, surge, sway and yaw wave-drift force components in body frame
H^e, H^s, H^L = exact, equivalent-linear and linear transfer functions of vessel motion responses
I_{zz} = vessel moment of inertia in yaw motion
L = ship length
m = vessel mass
$[m_{ij}]$ = 3*3 matrix of vessel mass
N, N_0 = yaw moment in body frame and natural equilibrium frame
$P(t,\gamma)$ = oscillatory wave-drift force with components (P_x, P_y, P_ψ) in body frame
$Q(t)$ = standard random excitation signal derived from $U(\mu)$
Q_0 = amplitude of standard harmonic excitation signal
r = moment arm of linear yaw moment
$r_e(t)$ = exact radial motion record
$r_0(t)$ = approximate radial motion record
$[R_{G_0}]$ = vector of vessel shift from global to natural equilibrium frame with components $(x_{G_0}, y_{G_0}, \psi_{G_0})$
$[R_{0_E}]$ = vector of vessel shift from natural equilibrium frame to equilibrium frame with components $(x_{0_E}, y_{0_E}, \psi_{0_E})$
R = mooring restoring force
R_x, R_y, R_ψ = components of R in body frame
$R_{x_0}, R_{y_0}, R_{\psi_0}$ = components of R in natural equilibrium frame
t = time
T = mooring line tension
T_{BR_i} = breaking strength of ith segment of mooring line
$[T_{ij}]$ = 3*3 matrix of characteristics of linear equations of motion
U_k, V_k = horizontal and vertical spans of kth mooring line
$U(\mu)$ = white band-limited unit one-sided spectrum
x, y, z = body frame axes
x_G, y_G, z_G = global frame axes
x_E, y_E, z_E = equilibrium frame axes
x_0, y_0, z_0 = natural equilibrium frame axes
$\bar{x}_0, \bar{y}_0$ = mean values of $x_0(t)$ and $y_0(t)$
X, Y, N = body forces in body frame
X_0, Y_0, N_0 = body forces in natural equilibrium frame
β = wave direction in natural equilibrium frame
β_c = current direction in natural equilibrium frame
β_w = wind direction in natural equilibrium frame
γ = wave direction in body frame
γ_c = current direction in body frame
γ_w = wind direction in body frame
Δ = vessel displacement
Δt = time interval
ω = frequency in the high-frequency region
μ = frequency in the low-frequency region
μ_{max} = cutoff frequency of white excitation spectrum
ρ = water density
$[\sigma_{ij}^2]$ = 3*3 covariance matrix
$\psi, \psi_G, \psi_E, \psi_o$ = yaw motion in body, global, equilibrium and natural equilibrium frames
ψ_{G_o}, ψ_{o_E} = see x_{G_o} and x_{o_E}
Φ = disk vessel diameter
Ω_k = direction of kth mooring line in body frame

the system, and this is a source of nonlinearity.

The ship and disk types of the vessel have been selected for two reasons. Firstly, the weather forces on disks are independent of the disk angular orientation in the horizontal plane while the forces on ships are so dependent. This requires different nonlinear mathematical models to be applied to the vessels, and by comparing their behavior it is possible to diagnose the nonlinearities in the ship case. Secondly, the two vessel types practically cover the area of interest, since the other generic hull forms (semisubmersible, spar buoy, sphere and submersible) are less suited for the deepwater mooring applications because of their low hydrostatic restoring forces.

The dynamics of the system include the mean and oscillatory excitations and responses of the vessel and the mooring system. The vessel responses are defined in terms of horizontal motions and the mooring system responses by the distribution of tensions and motions of the mooring line elements. The vessel and the moorings constitute a coupled system with practically an infinite number of degrees of freedom. Fortunately, it has been shown in [2] that the resonance frequencies of the mooring line parameters occur on practical installations outside of the low-frequency range; therefore the dynamics of the mooring system can be approximated here by a quasi-static model. This enables a description of the total system dynamics by the equations of the vessel motions only. The effect of the moorings on the vessel can therefore be represented by the restoring forces and by algebraic contributions to the excitation, damping and inertia terms in the equations of the vessel motion. Also, in the quasi-static model all mooring line parameters are uniquely related to the instantaneous orientation of the vessel in space; therefore they can all be determined as functions of the vessel motions. This model has been adopted in the present analysis.

Three complete theories are derived for predicting the low-frequency dynamics: nonlinear, linear, and simple static, the latter being a by-product of the linear model. The nonlinear theory presents solutions in the time domain by simulation. It is relatively expensive in terms of computer cost and therefore it is of limited use in routine design applications. A simpler and less expensive (but also less accurate) linear theory is derived too, and its limitations are evaluated. The linear theory is handled in the frequency domain. The static model is also evaluated since it is still the most popular tool in the industry and its validity has not been completely evaluated, to the authors' knowledge.

Ideally, solutions of nonlinear equations of motions should be solved analytically in the frequency domain, and by simulation in the time domain, since the two methods supplement one another. The present nonlinear theory utilizes the time-domain solutions only. It is particularly suited to the present applications for two reasons. Firstly, the nonlinear restoring forces are determined numerically only, and they can be handled directly in this form in the time domain. Secondly, the coding of the equations of motion alone is relatively trivial in this method and the higher-order terms of the expansions of various forces can be easily added to the equations in the future, as knowledge of such terms becomes available. In other words, it is a simple matter to raise the order of the theory without having to solve the problem anew. The disadvantage of the method is the relative lack of generality of the solutions—they are valid only for one particular set of input conditions at a time; thus many simulations must be performed to obtain a complete picture of the problem. This may sometimes become prohibitive in terms of computing costs. It is demonstrated, however, that this method can yield an almost complete matrix of results necessary for both design applications and a general understanding of the physical problem. The exception is the problem of stability in the narrow sense, that is, an unlimited growth of oscillations. The simulation is only capable of detecting the instability, if any, for a particular set of conditions, by a trial-and-error process, and in general it is difficult to guess the conditions that may yield instabilities when the equations of motion are nonlinear. Fortunately, if the past operational experience is any guide, the instability does not occur in the mooring applications. No case of it has ever been documented in over 20 years of offshore operations in all kinds of weather conditions. It should be pointed out that the instability in the wide sense (growing but bounded oscillations induced by excessive loads and causing the system failure) has occurred on many occasions, but this is a trivial mathematical case and it can be detected easily by the present theories. The feasibility and practicality of solving the nonlinear equations of motion by analytical methods in the frequency domain are addressed in [3]. It is concluded there that such procedures are not practical because of the complexity and lack of generality of the terms approximating the mooring restoring forces in the equations of motion.

The general philosophy adopted to this mooring problem is governed by accuracy and computing time considerations as well as by the usefulness of the end product to the mooring design applications. Accuracy must be regarded in the context of several inherent uncertainties always present in the mooring design (in addition to those related to the seakeeping problem), as follows. The theories assume a perfect geometry of the mooring system, which is rarely accomplished in real life. The topography of the sea bottom is difficult and costly to measure and it affects the vessel performance significantly. For example, a single undetected rock on the bottom may entangle a mooring line, thus affecting the line geometry. This may cause the line to carry most of the total load and the other lines to be slack. The anchors are typically dropped by workboats and their fall is not vertical due to water currents and because they are attached to the mooring lines, and therefore their positions on the bottom are rarely known accurately. The deck arrangements of the offshore exploration vessels are typically very complex with large windage areas; therefore the prediction of the wind loads is rarely accurate. Even if wind tunnel tests are performed, the error can be large because of the scaling errors.

Different but also significant inaccuracies are inherent in the model tests of moored vessels. The deepwater moorings cannot be accurately simulated in the model scale because of the limited tank depth and also because the mooring line dynamics are subject to different scaling laws than those of the vessels. It is difficult to simulate the wind, current, and wave effects simultaneously, and the first two may also strongly affect the total performance. Significant uncertainties also appear on the mathematical side of the problem. The present theories of the drift force are typically in error of 20 to 40 percent, or more. The theoretical knowledge of many high-order terms in the expansion of the equations of motion is quite limited and the experiments are either impractical or costly.

Taking into consideration these uncertainties and the objective to develop practical tools for mooring design applications, it seemed justified to introduce simplifications in the mathematics when it was obvious that the rigorous methods, although feasible, would extend the computing time by order(s) of magnitude. This refers to treating the mooring lines quasi-statically in two-dimensional form and to decoupling the dependence of the drift forces on the wave angle from that on the wave frequency. Both the treatment of the line dynamics three-dimensionally and rigorous drift force calculations would require massive computations, as can be noted from references [2] and [4], respectively. Due to the present simplifications, the complete theories could be developed in the form of self-contained algorithms with realistic computing times.

In order to make the present theories directly applicable to the design, the dynamic responses are computed in statistical and probabilistic terms. To obtain these results from the nonlinear simulations it is necessary only to generate random response signals and to measure the probabilities and statistics directly in the time domain. In order to compare the linear and nonlinear

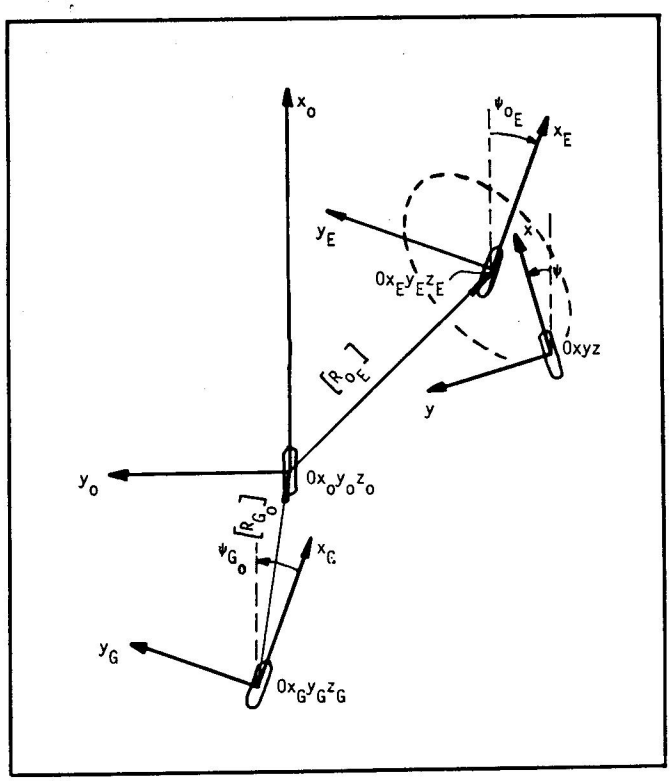

Fig. 2 Frames of reference

results, however, a spectral analysis of the nonlinear records is performed, and the derived spectra and transfer functions are compared with those of the linear theory and computed directly in the frequency domain. The spectra and transfer functions are also much more convenient for identification and diagnosis of the nonlinear phenomena. Also for this purpose, two additional types of simulations are performed: with regular harmonic excitation, which yields the nonlinear transfer functions, and with a square-wave excitation for examining the transient states of the system.

The mathematical models are presented as follows. Sections 2 to 4 describe the nonlinear theory with derivations of the equations of motion and of the excitation and restoring forces, respectively. Section 5 presents a description of the processing of the simulated nonlinear records in the time and frequency domains. Section 6 contains derivations of the dynamic linear and static theories. Finally, Sections 7 and 8 present results and conclusions, respectively.

It is concluded in the results that the static theory is inadequate on its own. The linear theory is valid for the case of the horizontal motions not exceeding 4 to 8 percent of water depth, for the vessels having the fairleads located sufficiently far from the center of gravity, as is the case in a typical drilling rig. For the analysis of larger motions or for the turret configurations of fairleads, the nonlinear theory should be used. Ships with turrets can experience violent motions with large feedback effects. The remaining nonlinearities are weak.

2. Equations of motion

Four frames of reference are utilized in formulating the equations of horizontal vessel motion. In each frame the motion is described by two orthogonal translations called surge (x or 1) and sway (y or 2), and a rotation, yaw (ψ or 3). All frames are right-handed, with x-y planes parallel to the mean sea level, with the z-axis pointing vertically upward, and initially all having the origins at the vessel center of gravity. The frames are shown in Fig. 2, and are defined as follows.

Global frame $Ox_Gy_Gz_G$ and natural equilibrium frame $Ox_oy_oz_o$. A vessel upon arrival at the mooring station has its anchors taken by a workboat and dropped at some specified positions. The vessel shifts during the drop and setting. Once all anchors and pre-tensions are set, the vessel takes a position of equilibrium of the mooring forces, in the absence of the weather elements. If the sea floor is irregular and the mooring system asymmetry is significant, the static displacement can be large. It is convenient from the operational point of view to know the total displacement vector and to prescribe accordingly the initial vessel position relative to the desired anchor positions. Two frames are used for this purpose, global frame (GF) and natural equilibrium frame (NEF), corresponding to the initial and final vessel positions, respectively. The initial position relative to the anchors is defined by the horizontal spans of the lines. The static displacemement vector, denoted $[R_{G_o}]$ has components

$$[R_{G_o}] = (x_{G_o}, y_{G_o}, \psi_{G_o}) \tag{1}$$

where ψ_{G_o} represents the vessel rotation. The global frame is used only once in a given problem. After computing the coordinates of the NEF, the anchor coordinates defined initially in the GF ($B_{x_{Gi}}, B_{y_{Gi}}, B_{z_{Gi}}$, i = line index) are recomputed in the NEF and the GF is no longer needed. The new anchor coordinates are

$$\begin{aligned} B_{x_{oi}} &= B_{x_{Gi}} \cos\psi_{G_o} + B_{y_{Gi}} \sin\psi_{G_o} - x_{G_o} \\ B_{y_{oi}} &= -B_{x_{Gi}} \sin\psi_{G_o} + B_{y_{Gi}} \cos\psi_{G_o} - y_{G_o} \\ B_{z_{oi}} &= B_{z_{Gi}} \end{aligned} \tag{2}$$

Equilibrium frame $Ox_Ey_Ez_E$. When the dc weather loads are applied, the vessel drifts to another position of static equilibrium. The frame attached to the vessel in the new position is named the equilibrium frame (EF). This frame is convenient for formulating the linear equations of the relative vessel motions, where the motions are assumed infinitesimal. The static displacement from $O_{x_oy_oz_0}$ to $O_{x_Ey_Ez_E}$ is defined by the vector

$$[R_{o_E}] = (x_{o_E}, y_{o_E}, \psi_{o_E}) \tag{3}$$

Although only the dc weather components are used for computing $[R_{o_E}]$, they are not constant on ships since they vary with the angle of incidence of the weather elements relative to the ship centerline.

Body frame O_{xyz}. The body frame, being fixed to the vessel at all times, is utilized for computing the inertia, damping, and excitation forces in the nonlinear equations of ship motions. This frame is not needed in the disk case since the body forces can be found directly in the NEF due to the disk symmetry.

It is the absolute vessel motions which are of interest in mooring applications; therefore all results of the nonlinear theory will be obtained by integrations in the NEF. Similarly, the results of the linear theory, although computed in the EF, will be converted to the NEF.

The time-domain integration requires that the highest derivatives of the motions be expressed explicitly. Therefore the following derivations lead to the motion accelerations in the NEF and, in the ship case, also to the auxiliary accelerations in the BF.

General equations in NEF. The Newtonian equations of the vessel motion are in this frame

$$\begin{aligned} m\ddot{x}_o &= X_o \\ m\ddot{y}_o &= Y_o \\ I_{zz}\ddot{\psi}_o &= N_o \end{aligned} \tag{4}$$

where m is the vessel mass, I_{zz} the mass moment of inertia about the z_o-axis; $\ddot{x}_o$, $\ddot{y}_o$, and $\ddot{\psi}_o$ the accelerations in surge, sway, and yaw; and X_o, Y_o, and N_o represent the total of excitations and body force components.

Equations of motion in BF (ship only). Performing the classical axis transformation [5,1], on the forces (X_o,Y_o,N_o) and accelerations $(\ddot{x}_o,\ddot{y}_o,\ddot{\psi}_o)$, the Newtonian equations in the BF become

$$\begin{aligned} m(\ddot{x} - \dot{y}\dot{\psi}) &= X \\ m(\ddot{y} - \dot{x}\dot{\psi}) &= Y \\ I_{zz}\ddot{\psi} &= N \end{aligned} \tag{5}$$

where the terms $m\dot{y}\dot{\psi}$ and $m\dot{x}\dot{\psi}$ represent the centrifugal forces. The right-hand sides of (5) are expanded in the Appendix into the excitation E, damping D, acceleration A, and restoring mooring forces R, as follows

$$X_i = E_i(t) - A_i(\ddot{x},\ddot{y},\ddot{\psi}) - D_i(\dot{x},\dot{y},\dot{\psi}) - R_i(x,y,\psi), \qquad X_i = X,Y,N \tag{6}$$

where the suffix $i = x,y,\psi$ denotes the three force components. The acceleration and damping forces are expanded further in the Appendix as explicit functions of the accelerations and velocities

$$A_i(\ddot{x},\ddot{y},\ddot{\psi}) = a_{i1}\ddot{x} + a_{i2}\ddot{y} + a_{i3}\ddot{\psi} \tag{7}$$

$$D_i(\dot{x},\dot{y},\dot{\psi}) = b_{i1}\dot{x} + b_{i2}\dot{y} + b_{i3}\dot{\psi} + c_{i1}\dot{x}^3 + c_{i2}\dot{y}^3 + c_{i3}\dot{\psi}^3 + c_{i4}\dot{y}\dot{\psi} \tag{8}$$

$$i = x,y,\psi = 1,2,3$$

The matrices of the added mass $[a_{ij}]$ and linear and higher-order damping terms $[b_{ij}]$ and $[c_{ij}]$ are defined in the Appendix. The excitation and mooring forces are derived in Sections 3 and 4, respectively, in both the BF (for the ship) and NEF (for the disk).

Substituting equations (6), (7) and (8) into equation (5) and reordering terms so that only the acceleration terms remain on the left-hand sides yields

$$\begin{aligned} (m + a_{11})\ddot{x} + a_{12}\ddot{y} + a_{13}\ddot{\psi} &= m\dot{y}\dot{\psi} + E_x(t) - D_x - R_x \\ a_{21}\ddot{x} + (m + a_{22})\ddot{y} + a_{23}\ddot{\psi} &= -m\dot{x}\dot{\psi} + E_y(t) - D_y - R_y \\ a_{31}\ddot{x} + a_{32}\ddot{y} + (I_{zz} + a_{33})\ddot{\psi} &= E_\psi(t) - D_\psi - R_\psi \end{aligned} \tag{9}$$

Before solving (9) algebraically for the accelerations, the terms which are always zero are eliminated to shorten the notation. It is shown in the Appendix that the terms with indices 12, 21, 13, and 31 are zero for the ship. The desired expressions for the accelerations in the BF become now

$$\begin{aligned} \ddot{x} &= [m\dot{y}\dot{\psi} + E_x - D_x - R_x]/(m + a_{11}) \\ \ddot{y} &= [(I_{zz} + a_{33})(-m\dot{x}\dot{\psi} + E_y - D_y - R_y) - a_{23}(E_\psi - D_\psi - R_\psi)]/M \\ \ddot{\psi} &= [-a_{32}(-m\dot{x}\dot{\psi} + E_y - D_y - R_y) + (m + a_{22})(E_\psi - D_\psi - R_\psi)]/M \end{aligned} \tag{10}$$

where

$$M = (m + a_{22})(I_{zz} + a_{33}) - a_{23}a_{32}$$

The sequence of operations for the ship is as follows. At any given time t, the NEF motions (x_o,y_o,ψ_o) and velocities $(\dot{x}_o,\dot{y}_o,\dot{\psi}_o)$ are available either from the initial conditions or from the last integration step. The motions serve to compute the restoring forces R. The yaw motion, together with the time t, serves to find the excitation forces E. The velocities are converted to the BF, $(\dot{x},\dot{y},\dot{\psi})$, and these serve to calculate the damping and centrifugal forces in equations (10). Having all terms in (10) available, the accelerations $(\ddot{x},\ddot{y},\ddot{\psi})$ are found and are converted to the NEF accelerations, $(\ddot{x}_o,\ddot{y}_o,\ddot{\psi}_o)$. The latter, together with velocities $(\dot{x}_o,\dot{y}_o,\dot{\psi}_o)$ and a desired time step Δt, serve as input to the next integration step.

The foregoing procedure could also be applied to the disk; however, it would be wasteful since all disk forces are available directly in the NEF. The disk equations are therefore reformulated.

Equations of motion in NEF (disk only). The forces on the right-hand sides of (4) are taken as being equal to (6), and in turn, to (7) and (8), but written with subscript o to denote that they are found directly in the NEF. Next, taking the terms with the highest derivatives to one side, eliminating the terms with subscripts 12, 21, 13, 31, 23, and 32, which are always zero on disks, and solving algebraically for the accelerations yields

$$\begin{aligned} \ddot{x}_o &= (E_{x_o} - D_{x_o} - R_{x_o})/(m + a_{11}) \\ \ddot{y}_o &= (E_{y_o} - D_{y_o} - R_{y_o})/(m + a_{22}) \\ \ddot{\psi}_o &= (E_{\psi_o} - D_{\psi_o} - R_{\psi_o})/(I_{zz} + a_{33}) \end{aligned} \tag{11}$$

Solutions of nonlinear equations of motion. There exists a multitude of published and well-proven algorithms for solving the ordinary differential equations. The code selected here utilizes the variable-step-size method where the step size is determined from the prescribed local-error limit and from the rapidity of changes of the functions being integrated. The code is described in a bulky but educational volume [6]. The principal advantage of this code is that it interpolates rather than evaluates the right-hand sides of the equations at most of the steps, provided the functions there are regular. Where some rapid variations occur in the functions, the step is decreased for an accurate integration. Both speed and accuracy are quite important in this problem since long records are required (of the order of several hundred motion cycles) in order to perform accurately the statistical analysis of the motion records.

The initial conditions have a strictly abstract meaning in the low-frequency problem because the always-present high-frequency motions serve as perturbations of the vessel path. Therefore the initial conditions are selected to shorten the computer time spent on handling the transient state; that is, they are chosen to be as close as possible to the low-frequency vessel path in the position-velocity space. The only point known *a priori* to lie close to it is the origin of the EF with zero velocities.[4]

3. Excitation forces

The excitation forces contain the mean and oscillatory parts of the wave force, denoted $\bar{E}$ and P, and the wind and current forces, F_w and F_c,

$$E_i(t,\gamma,\gamma_w,\gamma_c) = \bar{E}_i(\gamma) + P_i(t,\gamma) + F_{w_i}(\gamma_w) + F_{c_i}(\gamma_c), \qquad i = x,y,\psi \tag{12}$$

where

$$\begin{aligned} \gamma &= \beta - \psi_o(t) = \text{wave angle in BF} \\ \gamma_w &= \beta_w - \psi_o(t) = \text{wind angle in BF} \\ \gamma_c &= \beta_c - \psi_o(t) = \text{current angle in BF} \\ \beta,\beta_w,\beta_c &= \text{wave, wind and current angles in NEF} \end{aligned} \tag{13}$$

The implicit dependence of the forces on the yaw motion, $\psi_o(t)$, constitutes the yaw-excitation feedback phenomenon.

The wind and current vectors are assumed to be constant in time and the waves to be random and long-crested, defined by a spectrum $G_w(\omega)$.

The time signals of the second-order wave forces are derived in three steps. First, the forces in regular waves are determined in the form of nondimensional force and moment transfer functions. Next, the force component spectra are found from these and from the wave spectrum. Finally, the force component signals are obtained by a Fourier transformation.

Drift force transfer functions. A rigorous treatment of the forces in irregular waves presupposes a knowledge of the forces induced by two simultaneous regular-wave trains. Newman [7],

[4] This point is selected on a default basis. Optionally, arbitrary initial conditions can be selected.

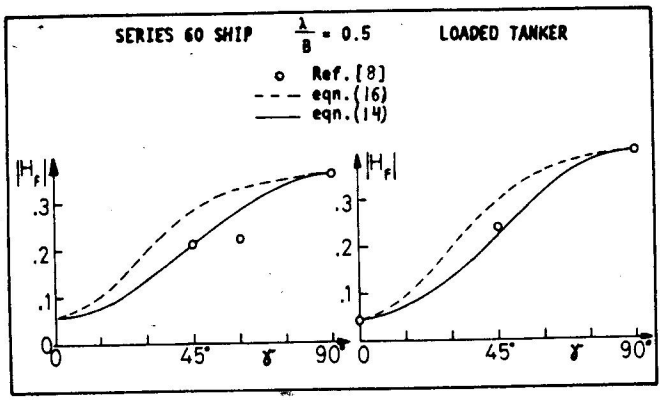

Fig. 3 Drift force dependence on wave angle in regular waves

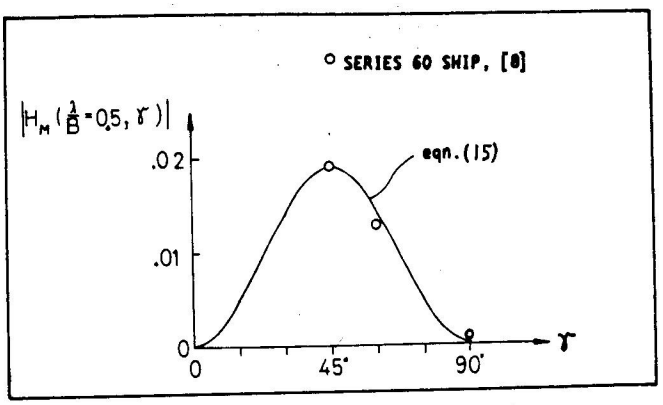

Fig. 4 Drift moment versus wave angle in regular waves

however, postulated that when the forces due only to a single harmonic train are utilized for the calculation of the force in irregular waves, the error will be small if the wave spectrum is narrow. This is an important aspect of the problem since there are no general methods of computing the double-frequency forces on 3-D bodies. Faltinsen [8] performed calculations of the forces on 2-D bodies in irregular waves based on rigorously derived double-frequency forces in regular waves and he compared them with Newman's approximation. The conclusion was that the approximation is fully justified for 2-D bodies and there is no reason to suspect that it would not hold for 3-D bodies. Therefore, in the present approach, the transfer functions of the forces are considered as being functions of a single frequency at a time.

The forces in regular waves are proportional to the wave amplitude squared, A^2, and they depend on the frequency ω, and in the ship case on the relative wave angle γ. A formal treatment of the dependence on γ requires separate and involved computation of the forces for each different γ. Since in the present problem the yaw motion is allowed to be large, the feedback introduces continuous and possibly large variations of γ; thus a rigorous derivation of the force signal would be impractical computationally. Therefore the dependence of the forces on γ is simplified, valid for slender ships, by decoupling it from the dependence on the frequency. The force is known to increase almost monotonically from bow-on to beam-on wave headings, and the moment increases from zero in head waves to a maximum in quartering waves and then back to almost zero in beam waves, and this behavior can be easily represented by curve fitting. The following expressions are used

$$H_F(\omega,\gamma) = \frac{\text{Force in wave direction}}{\rho g A^2 B} \cong H_F(\omega,0°)\cos^2\gamma + H_F(\omega,90°)\sin^2\gamma \quad (14)$$

$$H_M(\omega,\gamma) = \frac{\text{Moment}}{\rho g A^2 BL} \cong H_M(\omega,45°)\sin(-2\gamma)|\sin^2\gamma| \quad (15)$$

where B and L are the ship beam and length, and terms $H_F(\omega,0°)$, $H_F(\omega,90°)$ and $H_M(\omega,45°)$, given the names of generic forces, represent the force in head/stern and beam waves, and the moment in quartering waves, respectively. The generic forces are easier to compute than those in arbitrary oblique waves. Both (14) and (15) are applicable to all four quadrants of γ as the force magnitude on slender ships is symmetric with respect to the centerline and midship, and the yaw moment is always unstable. The quantity of the approximation (14) is demonstrated in Fig. 3, where it is compared with the exact values for a Series 60 ship and for a loaded tanker, both from [8]. Also shown in Fig. 3 is the curve fitting used in [9], as follows

$$H_F(\omega,\gamma) \cong H_F(\omega,0°)\frac{2\cos^2\gamma}{1+\cos^2\gamma} + H_F(\omega,90°)\frac{2\sin^2\gamma}{1+\sin^2\gamma} \quad (16)$$

The longitudinal and transverse components of the force in the BF are simply

$$H_{F_x}(\omega,\gamma) = H_F(\omega,\gamma)\cos\gamma$$
$$H_{F_y}(\omega,\gamma) = H_F(\omega,\gamma)\sin\gamma \quad (17)$$

A comparison of the approximation for the yaw moment, equation (15), with the few available results of Faltinsen [8] is shown in Fig. 4.

The force on the disk is independent of the wave angle, it acts in the wave direction, and the moment disappears since the disk is symmetrical. The force is nondimensionalized by $\rho g A^2 \Phi$ where Φ is the disk diameter.

The generic forces are obtained from an interpolating algorithm which uses as the data base the results available for 2-D cylinders [8] and empirical data for barges [10]. The force on ships in beam waves is found using strip theory, where the sectional forces are computed by triple interpolation of the Lewis section parameters (beam/draft ratio and area coefficient) and frequency. The longitudinal generic force is found by treating the entire ship as a single 2-D Lewis section and a correction for the block coefficient is applied to it. Also, the force on the disk is found by treating the disk as a single Lewis section with the walls subjected to a cube-into-disk transformation. The procedure is described and tested in [1]. It is shown that the final error is well within the error band of the rigorous methods. Figure 5 demonstrates it for a tanker, where the present results are shown by heavy lines and the dots and squares are from Faltinsen [8], who used the Newman/Helmholtz and Maruo expressions for the force.

The objective behind application of the preceding algorithm, in spite of the availability of rigorous methods [4,11,12], is that it allows the present mooring dynamics program to be self-contained, handled in its entirety with realistic computing times, while the rigorous methods are much more involved computationally and they do not seem to be much more accurate. They all suffer from a common defficiency of neglecting the viscous effects in evaluating the first-order motions, which serve, together with the first-order excitation, to obtain the second-order force. The symmetric motions are typically in error of up to 10 percent and the asymmetric ones up to 40 percent; thus the second-order forces are likely to carry an error of up to 40 percent too, as can be observed from a review of the most popular rigorous procedures in [8].

Drift force and moment spectra. There exist techniques for obtaining the force signals directly from the force transfer functions and wave spectrum or wave record [7,13]. In the present approach, an additional intermediate step is included of deriving first the force spectrum and then generating the signals from it by a Fourier transform. This approach is convenient for analyzing the feedback phenomena since the modulation of

the excitation by the feedback can be clearly observed in the spectra.

The mean values of the force, $\bar{E}$, and moment, $\bar{E}_\psi$, as well as the spectra of the force and moment, G_F and G_M, respectively, are derived in [1] using the method given in [14] in the form

$$\bar{E}(\gamma) = \rho g B \int_0^\infty G_w(\omega) H_F(\omega,\gamma) d\omega$$

$$\bar{E}_\psi(\gamma) = \rho g B L \int_0^\infty G_w(\omega) H_M(\omega,\gamma) d\omega \qquad (18a)$$

$$G_F(\mu,\gamma) = 2(\rho g B)^2 \int_0^\infty G_w(\omega) G_w(\omega+\mu) H_F^2\left(\omega + \frac{\mu}{2}, \gamma\right) d\omega$$

$$G_M(\mu,\gamma) = 2(\rho g B L)^2 \int_0^\infty G_w(\omega) G_w(\omega+\mu) H_M^2\left(\omega + \frac{\mu}{2}, \gamma\right) d\omega \qquad (18b)$$

where μ is the subfrequency, assumed in the derivations to be small, and $G_w(\omega)$ is the wave spectrum, assumed to be narrow.

When the moored vessels are large, their natural frequencies in the horizontal motions are small and the spectra (18*b*) need to be evaluated at only small frequencies μ. In this case, the double convolutions can be approximated by simple integrals by neglecting the dependence on μ. This results in the force spectra becoming band-limited white spectra

$$G_F(\mu,\gamma) = 2(\rho g B)^2 \int_0^{\mu_{max}} G_w^2(\omega) H_F^2(\omega,\gamma) d\omega = G_F^0(\gamma)$$

$$= \text{const in } \gamma \qquad (19a)$$

$$G_M(\mu,\gamma) = 2(\rho g B L)^2 \int_0^{\mu_{max}} G_w^2(\omega) H_M^2(\omega,\gamma) d\omega = G_M^0(\gamma)$$

$$= \text{const in } \gamma \qquad (19b)$$

$0 < \mu \leqslant \mu_{max}$, small

These expressions over estimate the force spectrum and the error increases with frequency. Therefore, the smaller the vessel, the more conservative will be the evaluation of the oscillatory drift force. A sensitivity analysis has been performed in [1] to examine this error, and also the effect of μ_{max} on the motions and the effect of the wave spectrum width. The following conclusions are extracted from it.

(*a*) Standard wave spectra can be used in expressions (18) and (19) with confidence. Four of them were examined: Bretschneider's, International Ship Structures Congress (ISSC), Pierson-Moskowitz's, and JONSWAP. The first three are relatively wide, and the JONSWAP is narrow as the assumption requires. The latter appears unacceptable, precisely because of this narrowness, since it magnifies the local errors which are always present in the force transfer functions. The ISSC turned out to be the most suitable. Being a two-parameter spectrum it yields good control over the spectrum shape and it is free of the deficiencies of the older two-parameter Bretschneider's spectrum. The one-parameter Pierson-Moskowitz spectrum is not recommended.

(*b*) The frequency cutoff, μ_{max}, equal to 150 percent of the maximum frequency of motion resonance is sufficient for motion simulation since the motion transfer functions have high peaks and they fall off rapidly at higher frequencies.

(*c*) The white-spectrum approximation yields negligible errors in large installations of practical interest.

Following the foregoing conclusions, the present method uses the ISSC wave spectrum. The white force spectrum has the frequency cutoff at 150 percent of the maximum natural frequency of the motions.

Substituting the transfer functions (14) and (15) into (19) and carrying our integrations yields

$$\bar{E}(\gamma) = \bar{E}(0°)\cos^2\gamma + \bar{E}(90°)\sin^2\gamma \qquad (20)$$

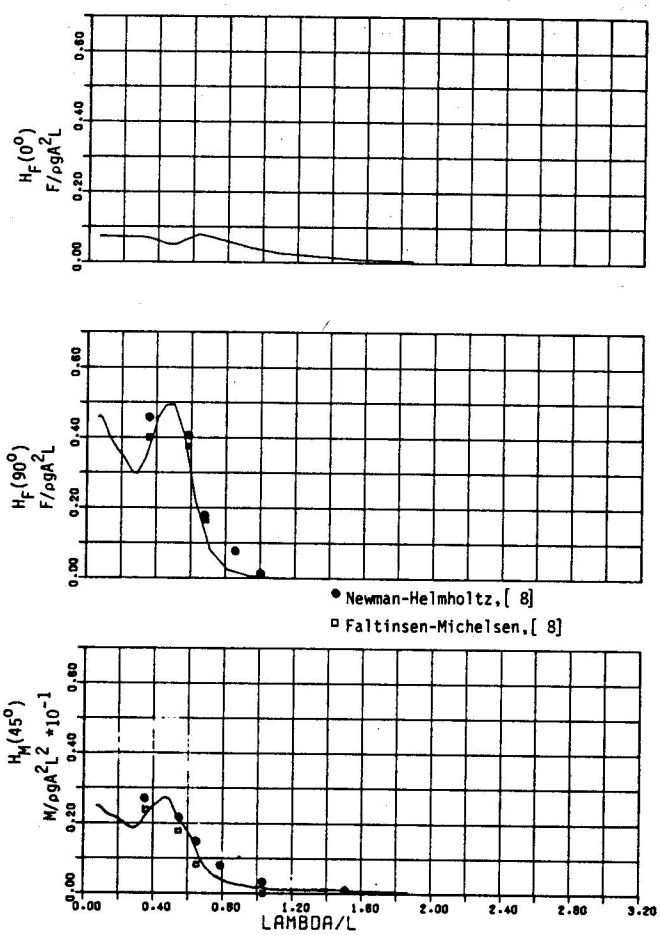

Fig. 5 Drift force transfer functions (generic), loaded tanker

$$\bar{E}_\psi(\gamma) = \bar{E}_\psi(45°)\sin(-2\gamma)|\sin 2\gamma| \qquad (21)$$

$$G_M^0(\gamma) = G_M^0(45°)\sin^4(2\gamma) \qquad (22a)$$

$$G_F^0(\gamma) = 2(\rho g B)^2 \int_0^{\mu_{max}} G_w^2(\gamma) H_F^2(\omega,\gamma) d\omega$$

$$= 2(\rho g B)^2 \int_0^{\mu_{max}} G_w^2(\gamma) H_F^2(\omega,0°) d\omega \cos^4\gamma$$

$$+ 2(\rho g B)^2 \int_0^{\mu_{max}} G_w^2(\gamma) H_F^2(\omega,90°) d\omega \sin^4\gamma$$

$$+ \left[2(\rho g B)^2 \frac{1}{2} \int_0^{\mu_{max}} G_w^2(\gamma) H_F(\omega,0°) H_F(\omega,90°) d\omega\right] \sin^2 2\gamma$$

Denoting the quantity in square brackets by G_P^0, the force spectrum becomes

$$G_F^0(\gamma) = G_F^0(0°)\cos^4\gamma + G_F^0(90°)\sin^4\gamma + G_P^0 \sin^2 2\gamma \qquad (22b)$$

Drift-force time signals. All spectra on the right-hand sides of (22) are white and all cover the same frequency range; therefore they all can be expressed as products of a standad unit white spectrum

$$U(\mu) \equiv 1 \quad 0 < \mu \leqslant \mu_{max}$$

and constant scaling factors, as follows

$$\begin{aligned} G_F^0(0°,\mu) &= G_F^0(0°)U(\mu) \\ G_F^0(90,\mu) &= G_F^0(90)U(\mu) \\ G_P^0(\mu) &= G_P^0 U(\mu) \\ G_M^0(\mu) &= G_M^0(45°)U(\mu) \end{aligned} \qquad (23)$$

Let the standard signal in time corresponding to the unit spectrum $U(\mu)$ be $Q(t)$.[5] It can be shown from the Fourier transform theory that if the spectral ordinates are multiplied by a constant C, then the signal ordinates must be multiplied by $C^{1/2}$ in order to preserve the transformation. Utilizing this fact, the oscillatory drift force components $P(t,\gamma)$ in equation (12) can be written as

$$P(t,\gamma) = \sqrt{G_F^0(\gamma)}\, Q(t) \tag{24}$$

Substituting (22*b*) into (24) yields the desired expression for the slowly oscillatory part of the force on ships

$$P(t,\gamma) = [G_F^0(0°)\cos^4\gamma + G_F^0(90°)\sin^4\gamma + G_P^0 \sin^2 2\gamma]^{0.5} Q(t) \tag{25}$$

The drift yaw moment is obtained similarly

$$P_\psi(t,\gamma) = \sqrt{G_M^0(\gamma)}\, Q(t) = \sqrt{G_M^0(45°)}\sin^2 2\gamma Q(t) \tag{26}$$

but there may exist in general a time shift between the force and moment, due to a phase shift between them in regular waves. However, since the spectra do not contain the phase information, the time shift must be selected arbitrarily. It is taken here as zero as it then yields the most conservative loading condition.

The decoupling of the dependence of the transfer functions on ω from that on γ, together with the white-spectrum approximations, yielded a considerably more efficient formulation of the oscillatory parts of the forces. Firstly, only four simple integrals for $G_F^0(0°)$,$G_F^0(90°)$, G_P^0 and $G_M^0(45°)$ need be evaluated to completely describe the spectrum in arbitrary wave headings versus the more involved double convolutions (18) which would have to be computed individually for each different wave angle. Secondly, only one Fourier transform is necessary, from $U(\mu)$ to $Q(t)$, and it is the same for all possible cases; thus it can be computed once, stored, and utilized in all applications.

The wave-force signal in the disk case follows from the ship case by omitting the dependence on wave angle. The mean force becomes

$$\overline{E} = \rho g \Phi \int_0^\infty G_w(\omega) H_F(\omega) d\omega \tag{27}$$

and the spectrum

$$G_F^0(\mu) = 2(\rho g \Phi)^2 \int_0^\infty G_w^2(\omega) H_F^2(\omega) d\omega = \text{const} = G_F^0 \qquad 0 < \mu \leq \mu_{max} \tag{28}$$

resulting in the following expression for the force signal

$$E(t) = \overline{E} + \sqrt{G_F^0}\, Q(t) \qquad E_\psi(t) \equiv 0 \tag{29}$$

Wind and current forces. The wind and current forces on ships are evaluated similarly to the mean wave forces in terms of the dependence on the incidence angle

$$F_i(\gamma_i) = F_i(0°)\cos^2\gamma_i + F_i(90°)\sin^2\gamma_i$$
$$\begin{Bmatrix} F_{i_x}(\gamma_i) \\ F_{i_y}(\gamma_i) \end{Bmatrix} = F_i(\gamma_i) \begin{Bmatrix} \cos\gamma_i \\ \sin\gamma_i \end{Bmatrix} \tag{30}$$
$$F_{i_\psi}(\gamma_i) = F_{i_\psi}(45°)\sin(-2\gamma)|\sin 2\gamma_i|$$

where $i = w$ for wind or $i = c$ for current, and where the force components are expressed in the BF.

The forces on disks are independent of the incidence angle. They become in the NEF

$$F_i = F = \text{const}$$
$$\begin{Bmatrix} F_{i_{x_o}} \\ F_{i_{y_o}} \end{Bmatrix} = F \begin{Bmatrix} \cos\beta_i \\ \sin\beta_i \end{Bmatrix} \tag{31}$$
$$F_{i_{\psi_o}} \equiv 0$$

where $i = w$ or c, as before.

Total excitation forces. Summing up the wind, current, and mean and oscillatory wave forces yields the final force components in the BF due to a random environment

$$\begin{Bmatrix} E_x(t,\gamma) \\ E_y(t,\gamma) \end{Bmatrix} = [\overline{E}(0°)\cos^2\gamma + \overline{E}(90°)\sin^2\gamma] \begin{Bmatrix} \cos\gamma \\ \sin\gamma \end{Bmatrix}$$
$$+ [F_w(0°)\cos^2\gamma_w + F_w(90°)\sin^2\gamma_w] \begin{Bmatrix} \cos\gamma_w \\ \sin\gamma_w \end{Bmatrix}$$
$$+ [F_c(0°)\cos^2\gamma_c + F_c(90°)\sin^2\gamma_c] \begin{Bmatrix} \cos\gamma_c \\ \sin\gamma_c \end{Bmatrix}$$
$$+ [G_F^0(0°)\cos^4\gamma + G_F^0(90°)\sin^4\gamma + G_P^0 \sin^2 2\gamma]^{0.5} Q(t) \begin{Bmatrix} \cos\gamma \\ \sin\gamma \end{Bmatrix} \tag{32a}$$

$$E_\psi(t,\gamma) = \overline{E}(45°)\sin(-2\gamma)|\sin 2\gamma| + F_w(45°)\sin(-2\gamma_w)|\sin 2\gamma_w| + F_c(45°)\sin(-2\gamma_c)|\sin 2\gamma_c| + \sqrt{G_M^0(45°)}\sin^2 2\gamma Q(t) \tag{32b}$$

The excitation forces on the disk are summed up in the NEF

$$\begin{Bmatrix} E_{x_o}(t) \\ E_{y_o}(t) \end{Bmatrix} = \overline{E} \begin{Bmatrix} \cos\beta \\ \sin\beta \end{Bmatrix} + F_w \begin{Bmatrix} \cos\beta_w \\ \sin\beta_w \end{Bmatrix} + F_c \begin{Bmatrix} \cos\beta_c \\ \sin\beta_c \end{Bmatrix} + \sqrt{G_F^0} Q(t) \begin{Bmatrix} \cos\beta \\ \sin\beta \end{Bmatrix} \tag{33}$$
$$E_{\psi_o}(t) \equiv 0$$

The standard signal $Q(t)$ is generated at equal intervals $r \cdot \Delta t$, as $Q(t_r)$. Since the algorithm which integrates the non-linear equations of motion is of the variable-step-size type, the signal must be made available at any arbitrary time. The following interpolation is used for this purpose

$$Q(t) = \sum_{l=-4}^{4} \frac{\sin\frac{\pi}{\Delta t}(t - t_l)}{\frac{\pi}{\Delta t}(t - t_l)} Q(t_{r+l}) \qquad t_r < t \leq t_{r+1} \tag{34}$$

This expression preserves both the mean and root-mean-square (rms) values of the original signal. Its theory and evaluation are given in [16].

Regular excitation. For the case of a harmonic excitation, the random signal $Q(t)$ should be replaced by some harmonic $Q_o e^{i\omega t}$. If the system were linear, there would exist a unique set of the motion transfer functions, one per motion mode, each being independent of the magnitude of the oscillatory excitation; thus any value of Q_0 could then be used. In the nonlinear case, there may exist an infinite family of the transfer functions dependent parametrically on the excitation magnitude; thus in order to correlate the results obtained from the "random" and "regular" simulations, the two excitation magnitudes must be made equivalent in some sense. The criterion adopted here is to equate the energies of the random and harmonic signals

$$\int_0^{\mu_{max}} U(\mu) d\mu = \mu_{max} = \frac{Q_0^2}{2}$$

which yields the desired amplitude

$$Q_0 = \sqrt{2\mu_{max}}$$

[5] The most efficient method of obtaining $Q(t)$ from $U(\mu)$ is by using the Fast Fourier Transform [1,15], with the arbitrary phase angles being generated randomly from the uniform distribution between 0 and 2π, thus yielding a Gaussian signal $Q(t)$.

In the disk case, if $Q(t)$ is harmonic, the oscillatory excitation will be harmonic too. In the ship case, however, the oscillatory components may not be harmonic because of the feedback effect in equation (32).

4. Mooring restoring forces

When the vessel path is horizontal and when the mooring lines are constrained to vertical planes, the static loads and shapes of the lines are uniquely related to the horizontal spans of the lines. For a mooring line to take a 2-D shape in a vertical plane, the general external horizontal forces acting on the line must vanish. They include the current loads and the friction on the sea floor in the direction nonparallel to the line. The effect of these loads can be shown to be small in multileg moorings. It is significant only for the lightly loaded, slack lines, but its relative influence on taut lines is small. Since the taut lines contribute by far the most to the total horizontal force, the neglect of those loads causes small errors only.

It is theoretically possible to handle the 3-D shapes of the mooring lines using finite-element models, for example, [2], but it would obviously result in the simulation time being longer by order(s) of magnitude. Because of this, and in view of the small gains of accuracy that could be achieved, it is considered impractical. Instead, the much simpler catenary equations are used for the line mechanics. The assumption of 2-D shapes also permits us to reduce the simulation time further by presolving the line parameters for all possible systematically arranged horizontal line spans. Since the spans, being dependent on the vessel position, are known during the simulation, it is possible to compute the instantaneous line forces by interpolating on the spans. The table which contains the line parameters (including the horizontal and vertical tensions at fairleads) is named the Catenary Table.

The theory of the mooring line utilized here has been described in [22]. It is valid for any multisegment line of arbitrary composition of wires, chains, buoyant or neutrally buoyant or nonbuoyant synthetic ropes, and submerged and surface buoys. The anchor can lie on a sloping bottom and the synthetic ropes can be nonlinearly stretchable.

Total mooring restoring forces. The horizontal span of the kth line is available at any instant as a function of vessel motion (x_o, y_o, ψ_o), the anchor position, and the fairlead geometry

$$U_k = [(B_{x_{ok}} - A_{x_{ok}})^2 + (B_{y_{ok}} - A_{y_{ok}})^2]^{0.5}, k = 1, \ldots K \quad (35)$$

where

$B_{x_{ok}}, B_{y_{ok}}$ = kth anchor coordinates in NEF
$A_{x_{ok}}, A_{y_{ok}}$ = kth fairlead coordinates in NEF, given by the fairlead coordinates in BF and vessel motions, as follows

$$\begin{aligned} A_{x_{ok}} &= x_0 + A_{x_k} \cos\psi_0 - A_{y_k} \sin\psi_0 \\ A_{y_{ok}} &= y_0 + A_{x_k} \sin\psi_0 + A_{y_k} \cos\psi_0 \end{aligned} \quad (36)$$

The horizontal forces in the line plane, H_k, are available from the Catenary Table by interpolation on U_k. The total mooring forces in the BF (utilized in the ship motion equations) become

$$\begin{Bmatrix} R_x \\ R_y \end{Bmatrix} = \sum_{k=1}^{K} H_k \begin{Bmatrix} \cos \\ \sin \end{Bmatrix} \Omega_k \quad (37)$$

$$R_\psi = \sum_{k-1}^{K} H_k [\cos\Omega_k (A_{x_{ok}} - x_0) - \sin\Omega_k (A_{y_{ok}} - y_o)]$$

where Ω_k is the direction of the kth line in BF. The forces in the NEF (utilized for the disk) are

$$\begin{aligned} R_{x_o} &= R_x \cos\psi_o + R_y \sin\psi_o \\ R_{y_o} &= R_y \cos\psi_o - R_x \sin\psi_o \\ R_{\psi_o} &= R_\psi \end{aligned} \quad (38)$$

Figure 6 illustrates sample mooring force components R_{x_o}, R_{y_o}, and R_{ψ_o} for an asymmetric mooring system as "3-D" functions of the position x_o and y_o, with ψ_o = const = 0°.

5. Processing of time records

The simulated records are first processed to yield information which could be directly and exhaustively used in designs of mooring systems. This includes measurements of the probability density functions (PDF's), the mean and rms values of the excitations and responses, and χ-square tests of the probability that the PDF's are Gaussian. These results give the designer two choices. First, the Gaussianity can be accepted at some probability level. Then the mean and rms values can be utilized to formulate the theoretical normal and Rayleigh PDF's of the parameters to obtain all statistics of interest (typically the Nth highest responses) from the well-established formulas (for example, [19]). Alternatively, the Gaussianity can be rejected; then the statistics must be obtained numerically directly from the measured PDF's.

Also included in the record processing is an analysis of the sensitivity of the responses to weather conditions and mooring-system stiffness in a broad range of these parameters. This serves two purposes. Firstly, the results of the linear and nonlinear theories can be compared with each other to establish the envelope of validity of the former theory. Secondly, a general understanding of the nonlinear mooring phenomena is sought, and their importance in practical applications is assessed. The sensitivity analysis is based on transient-state simulations, on the transfer functions of the responses measured in the time domain

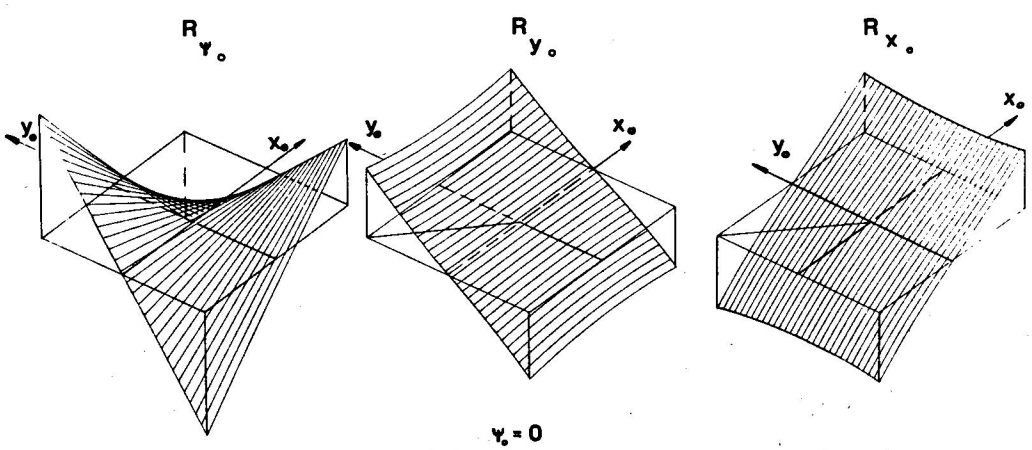

Fig. 6 Components of mooring restoring force as functions of vessel position, yaw (ψ_0) = 0

from regular records, and on a Fourier analysis of random records which yields spectra and equivalent-linear transfer functions (linearized in the least-square sense). These are compared with the spectra and linear transfer functions derived from the linear equations of motion directly in the frequency domain.

The transfer functions of the responses, although being informative in the sensitivity analysis, are of little use to the designer since they lack generality. Even if the system were perfectly linear, there would exist a separate set of the functions in each different weather condition because the effective mooring-system stiffness depends on the initial stiffness and on the stiffness changes induced by the mean weather loads.

The parameters obtained from the records are computed as follows.

(*a*) Probability density functions are measured using a probability analyzer [1,15] with 20 intervals spanning the parameter range, and based on 2400 samples of the steady-state part of the record. This number of samples is also used to measure the mean and rms values of the records.

(*b*) Exact transfer functions, of a response $x(t)$, have their modulas measured from the regular-excitation simulations as

$$|H_x^e(\omega)| = \left.\frac{[x(t)]_{\max} - [x(t)]_{\min}}{[E(t)]_{\max} - [E(t)]_{\min}}\right|_{\omega=\text{const}} \tag{39}$$

where $E(t)$ is the total excitation force signal. This expression gives the function value at one frequency only. A total of 17 frequencies is applied, one at a time, they are selected automatically in the neighborhood of the natural frequencies of the vessel motions, for detecting the jump phenomena, if any.

(*c*) The spectra of the excitations and responses are computed by the Fast Fourier Transform [15], using 800 samples, and 224 amended zeros per record. The Nyquist frequency corresponds in all cases to twice the maximum actual frequency of the system. A cosine window of the type (1/10, 8/10, 1/10) is applied to all records and a smoothing is performed to yield 25 degrees of freedom of the χ-square distribution.

(*d*) Equivalent-linear transfer function $H_x^s(\omega)$ of some response $x(t)$ is obtained for all motions, in the least-square sense, as

$$|H_x^s(\omega)| = \left[\frac{G_{xx}(\omega)}{G_{EE}(\omega)}\right]^{0.5} \tag{40}$$

where G_{xx} and G_{EE} are the response and total-excitation-force spectra, respectively.

(*e*) Transient-state records are obtained by simulating the motion of the vessel released from the EF origin and drifting to the NEF origin in the absence of weather elements. This is analogous to using a step excitation.

The statistical analysis, being based on single records, requires the assumption of stationarity and ergodicity. The stationarity has been verified by the trend tests [15], for all weather conditions and mooring-system stiffness combinations of practical interest, including the cases where nonlinearities are significant. The stationarity is, however, a necessary idealization here, since the real simulation time is typically 5 to 30 hours and the weather is most likely to vary during such a long time.

The basic set of records includes three excitation components, $E_{x_o}(t)$, $E_{y_o}(t)$, and $E_{\psi_o}(t)$, and three motion responses, $x_o(t)$, $y_o(t)$, and $\psi_o(t)$. Four additional records are derived from these, as follows.

The exact radial motion, $r_e(t)$, defined as

$$r_e(t) = [x_o^2(t) + y_o^2(t)]^{0.5} \tag{41}$$

is often desired in offshore applications for evaluating the stresses on underwater tools suspended off the vessel and attached to the sea bottom (for example, drill strings on drill ships). This record is used for measuring the PDF of the radius and its exact transfer function, $H_{r_e}^e(\omega)$. (The plots displayed later show this radius.) The definition (41) is, however, inconvenient to use for comparisons between the nonlinear and linear motions in the frequency domain since the spectrum of (41) has the frequency range doubled relative to that of either x_0 or y_0, whichever is greater, due to the squaring operation in (41), and the derivation of the spectrum from the linear surge and sway is cumbersome computationally. Therefore the comparison is performed on an approximate radius, which is free of this deficiency, and having the error so small in practical applications that the approximation can still be used as an estimate of $r_e(t)$. It is defined as the projection of $r_e(t)$ onto the line passing through the NEF origin and the mean vessel position $(\bar{x}_o, \bar{y}_o)$. The oscillatory part of this quantity, $r_o(t)$, is

$$\begin{aligned} r_o(t) &= r_L(t)\cos\theta(t) \\ r_L(t) &= \{[x_o(t) - \bar{x}_o]^2 + [y_o(t) - \bar{y}_o]^2\}^{0.5} \\ \theta(t) &= \tan^{-1}\frac{\bar{y}_o}{\bar{x}_o} - \cos^{-1}\frac{x_o(t) - \bar{x}_o}{r_L(t)} \end{aligned} \tag{42}$$

Since the vessel remains approximately the same amount of time inside and outside the mean radius circle, its harmonic range is almost the same as that of $x_o(t)$ and $y_o(t)$.

The modulus of the total excitation force signal, $|E(t)|$, is included to facilitate the detection of the force zero-crossings. Due to the always-present large mean force, the number of crossings is usually small and difficult to observe from the record. The modulus reverses the negative portions of the record, thus introducing superharmonics which can be easily detected in the spectrum.

All records considered so far describe the vessel dynamics only. In order to describe the mooring system parameters, the records of the line tensions at the fairleads, $T(t)$, are also included. Knowing the tensions, all other parameters of the mooring system can be obtained from the Catenary Table. When all mooring lines are identical and the sea floor is level, it is sufficient for design purposes to obtain one tension record only, that of the instantaneous tension occurring in the most loaded line. Thus this record is built of contributions of several, if not all, mooring lines.

The records, as well as the parameters derived from them (spectra, transfer functions, and probabilities) are displayed using the following non-dimensionalization

$E(t), \|E(t)\|, E_{x_o}(t)$ and $E_{y_o}(t)$	are divided by $\Delta/1000‰$
$E_{\psi_o}(t)$	is divided by $\Delta L/1000‰$
$x_o(t), y_o(t), r_e(t)$ and $r_o(t)$	are divided by $D/100\%$
$T(t)$	is divided by $T_{BR}(t)/100\%$
$\psi_o(t)$	is in degrees

where Δ, D, L, and T_{BR} are, respectively, the vessel displacement, water depth, ship length, and the breaking strength of the line on which the tension is measured.

6. Linear theory of low-frequency dynamics

When the oscillatory vessel motions about the EF origin are assumed to be infinitesimal, the equations of motion can be linearized about that origin and then they can be solved directly in the frequency domain in a manner similar to that used in the seakeeping theory. Such solutions are obviously much less involved computationally but their disadvantage, besides being less general, is that they yield directly only the vessel dynamics statistics and not those of the mooring system. In the nonlinear theory the instantaneous mooring line parameters are available at all times. In the present case they are not, because the linearized restoring force coefficients represent the combined contributions of all mooring lines and thus the information about the individual mooring lines is lost in the equations of the vessel motion. A direct linearization of the line parameters is obviously possible, but in view of their strongly nonlinear character, it would lead to inaccurate results. In contrast, the total mooring

forces can be linearized since the nonlinearities of the leeward and weather lines partly cancel each other out. Utilizing the quasi-static dependence of the lines parameters on the vessel motions, the parameters can be computed more accurately by finding the motions first and then extracting the mooring data from the Catenary Table by entering the table with the line spans computed from the motions.

The linearization is applied to the oscillatory relative vessel motions only. The static vessel shift $[R_{o_E}]$, equation (3), is still found exactly, that is, with the feedback effect present.

Linear equations of motion. These equations are obtained from the nonlinear equations (10) by dropping all nonlinear terms and linearizing the mooring forces about the EF origin. Subscript E is assigned to the variables defined in the EF. The result is

$$\sum_{j=1}^{3} [(m_{ij} + a_{ij})\ddot{x}_{E_j} + b_{ij}\dot{x}_{E_j} + d_{ij}x_{E_{ij}}] = E_{i_E}(t) \qquad (43)$$

$$x_{E_j} = x_E, y_E, \psi_E \qquad i = x,y,\psi = 1,2,3$$

where $[m_{ij}]$, $[a_{ij}]$, and $[b_{ij}]$ remain as before since the BF in which they were defined now coincides in angular orientation with the EF; $[d_{ij}]$ is the mooring stiffness matrix

$$d_{ij} = \left.\frac{\partial R_i}{\partial x_j}\right|_{x_E = y_E = \psi_E = 0} \qquad i,j = x_E, y_E, \psi_E$$

The oscillatory excitation forces on ships are obtained by dropping the steady forces $\overline{E}$, F_w, and F_c in equation (32) and by eliminating the feedback effect in view of the small motion assumption. That is, the steady yaw shift ψ_{o_E}, equation (3), is substituted for $\psi_o(t)$ in equation (13), causing the relative wave angle $\gamma(t)$ to become constant, $\overline{\gamma}$

$$\gamma(t) = \beta - \psi_o(t) \cong \beta - \psi_{o_E} = \overline{\gamma}$$

It follows that the force spectra (22) become constant too

$$G_F^0(\gamma) \cong G_F^0(0°)\cos^4\overline{\gamma} + G_F^0(90°)\sin^4\overline{\gamma} + G_P^0 \sin^2 2\gamma = G_F^0$$
$$G_M^0(\gamma) \cong G_M^0(45°)\sin^4 2\overline{\gamma} = G_M^0 \qquad (44)$$

The resultant excitation components are then, from (32) and (33):

$$\begin{Bmatrix} E_{x_E}(t) \\ E_{y_E}(t) \end{Bmatrix} = \sqrt{G_F^0}\, Q(t) \begin{Bmatrix} \cos\overline{\gamma} \\ \sin\overline{\gamma} \end{Bmatrix} = E_E(t) \begin{Bmatrix} \cos\overline{\gamma} \\ \sin\overline{\gamma} \end{Bmatrix}$$
$$E_\psi(t) = \sqrt{G_M^0} Q(t)$$

Let the moment be written as a product of the force $E_E(t)$ and an arm r

$$E_{\psi_E}(t) = rE_E(t) = [G_M^0/G_F^0]^{0.5} E_E(t)$$

Then all three excitation components on a ship can be written as

$$E_{i_E}(t) = \sqrt{G_F^0}\, Q(t) \begin{cases} \cos\overline{\gamma} & i = x \\ \sin\overline{\gamma}, & i = y \\ r & i = \psi \end{cases} \qquad (45)$$

The components on the disk are obtained similarly

$$E_{i_E}(t) = \sqrt{G_F^0}\, Q(t) \begin{cases} \cos\overline{\gamma} & i = x \\ \sin\overline{\gamma}, & i = y \\ 0 & i = \psi \end{cases}$$

where G_F^0 is in this case given by equation (28).

Since all three excitation components are now expressed as products of the drift force $E_E(t)$ and constant factors ($\sin\overline{\gamma}$, $\cos\overline{\gamma}$, r), the three-input model has been effectively reduced to a single-input one.

Let the standard signal $Q(t)$ be harmonic, $e^{i\omega t}$. Thus the steady-state linear responses are harmonic too

$$\begin{Bmatrix} x_E \\ y_E \\ \psi_E \end{Bmatrix} = \begin{Bmatrix} x_E^0 \\ y_E^0 \\ \psi_E^0 \end{Bmatrix} e^{i\omega t} \qquad (46)$$

with complex amplitudes x_E^0, y_E^0, and ψ_E^0. Substituting (45) and (46) into (43) and canceling $e^{i\omega t}$ yields

$$\sum_{j=1}^{3} [-(m_{ij} + a_{ij})\omega^2 + ib_{ij}\omega + d_{ij}]x_{E_j}^0 = |E_E| \begin{cases} \cos\overline{\gamma} & i = 1 \\ \sin\overline{\gamma} & i = 2 \\ r & i = 3 \end{cases} \qquad (47)$$

$$x_{E_j}^0 = x_E^0, y_E^0, \psi_E^0$$

The following substitutions are introduced

$$-(m_{ij} + a_{ij})\omega^2 + ib_{ij}\omega + d_{ij} = T_{ij} \qquad (48)$$

$$\frac{x_{E_i}^0}{|E_E|} = H_{j_E}(\omega) \qquad (49)$$

Dividing (47) by $|E_E|$ and utilizing (48) and (49) gives three algebraic equations for $H_{j_E}(\omega)$, $j = x,y,\psi$. Their solutions are

$$H_{x_E}(\omega) = \frac{1}{D}[\cos\overline{\gamma}(T_{22}T_{33} - T_{32}T_{23}) + \sin\overline{\gamma}(T_{13}T_{32} - T_{33}T_{12}) + r(T_{12}T_{23} - T_{22}T_{13})]$$

$$H_{y_E}(\omega) = \frac{1}{D}[\cos\overline{\gamma}(T_{23}T_{31} - T_{33}T_{21}) + \sin\overline{\gamma}(T_{11}T_{33} - T_{13}T_{31}) + r(T_{13}T_{21} - T_{23}T_{11})] \qquad (50)$$

$$H_{\psi_E}(\omega) = \frac{1}{D}[\cos\overline{\gamma}(T_{21}T_{32} - T_{31}T_{22}) + \sin\overline{\gamma}(T_{12}T_{31} - T_{32}T_{11}) + r(T_{11}T_{22} - T_{12}T_{21})]$$

where D is the determinant of the equations, $|T_{ij}|$.

The quantities $H_{j_{E(\omega)}}$ represent the complex transfer functions of the oscillatory surge, sway, and yaw motions in the EF. They are next transformed to the NEF components, denoted by superscript L (for linear)

$$\begin{aligned} H_{x_o}^L(\omega) &= H_{x_E}(\omega)\cos\psi_{o_E} - H_{y_E}(\omega)\sin\psi_{o_E} \\ H_{y_o}^L(\omega) &= H_{x_E}(\omega)\sin\psi_{o_E} + H_{y_E}(\omega)\cos\psi_{o_E} \\ H_{\psi_o}^L(\omega) &= H_{\psi_E}(\omega) \end{aligned} \qquad (51)$$

The natural frequencies of the linear surge, sway, and yaw motions are found by solving the following characteristic equations

$$T_{ii}(\omega_i) = 0 \quad i = 1,2,3, = x,y,\psi \qquad (52)$$

Linear radial motion. The surge and sway motions in the EF, due to the excitation of unit amplitude and frequency ω, can be written in the form

$$\begin{aligned} x_E^u(\omega t) &= |H_{x_E}| \cos\omega t \\ y_E^u(\omega t) &= |H_{y_E}| \cos(\omega t + \epsilon_y - \epsilon_x) \end{aligned} \qquad (53)$$

where ϵ_x and ϵ_y represent the phases contained in the transfer functions, u stands for the motion due to unit excitation, and where both motions are measured from the beginning of the surge motion cycle. The path (53) (shown in Fig. 7) is an ellipse. The points on the ellipse which are closest and farthest away from the Ox_oy_o origin, denoted C' and C, lie on the arcs described by $R_{\min}$ and $R_{\max}$. The intersection of the arcs with the line r_o is shown by points B' and B. When the oscillatory motions are small in comparison with the mean radius r_0, the arcs $R_{\min}$ and $R_{\max}$ can be locally approximated by straight lines, and the points B' and B can then be approximated by A' and A. The error of the approximation disappears, when one of the ellipse axis coincides

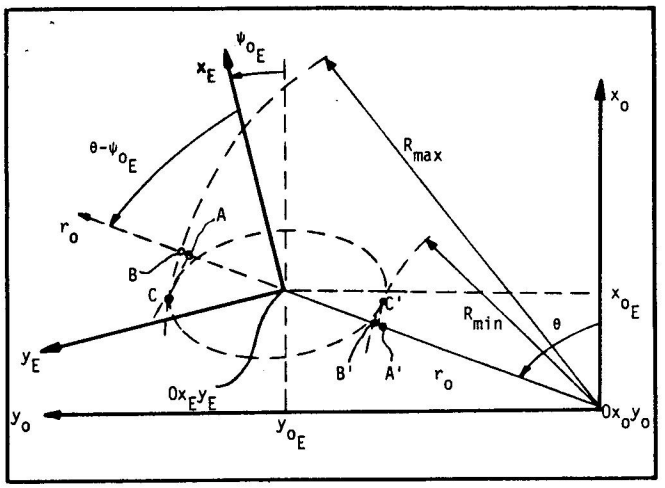

Fig. 7 Linear radial motion

with the line r_o, and this would be likely to occur when all weather components are nearly colinear. The angle between the x_E-axis and the direction r_o is $\theta - \psi_{o_E}$, where $\theta = \tan^{-1}(y_{o_E}/x_{o_E})$. The projection of the ellipse onto the line r_o is therefore given by the linear axis transformation

$$r^u = x_E^u \cos(\theta - \psi_{o_E}) + y_E^u \sin(\theta - \psi_{o_E})$$
$$= |H_{x_E}| \cos\omega t \cos(\theta - \psi_{o_E})$$
$$+ |H_{y_E}| \sin(\theta - \psi_{o_E}) \cos(\omega t + \epsilon_y - \epsilon_x) \quad (54)$$

The modulus of the radial-motion transfer function is given by the amplitude of r^u

$$H_{r_o}^L(\omega) = \max[r^u(\omega t)] \quad (55)$$

The time angle $\Omega = \omega t$ which maximizes $r^u(\omega t)$ is found by equating $\partial r^u(\omega t)/\partial(\omega t)$ to zero

$$\Omega|r_{max}^u = \tan^{-1}$$
$$\times \frac{-|H_{y_E}| \sin(\theta - \psi_{o_E}) \sin(\epsilon_y - \epsilon_x)}{|H_{x_E}| \cos(\theta - \psi_{o_E}) + |H_{y_E}| \sin(\theta - \psi_{o_E}) \cos(\epsilon_y - \epsilon_x)} \quad (56)$$

The desired transfer function thus takes the form

$$|H_{r_o}^L(\omega)| = \text{abs}\{|H_{x_E}(\omega)| \cos\Omega(\omega) \cos(\theta - \psi_{o_E})$$
$$+ |H_{y_E}(\omega)| \sin(\theta - \psi_{o_E}) \cos[\Omega(\omega)$$
$$+ \epsilon_y(\omega) - \epsilon_x(\omega)]\} \quad (57)$$

and the motion r_0 is harmonic with the same frequency ω as the linear surge and sway motions. The foregoing approximation obviates the need to consider the extended frequency range of the exact radial motion, $[x_E^2(t) + y_E^2(t)]^{1/2}$. Recall that the radius $r_0(t)$ derived from the nonlinear surge and sway is also defined in the same way, for consistency.

Probabilities and statistics. The cospectra of the linear surge, sway, and yaw motions are available from the classical expression

$$G_{ij}(\mu) = [H_i^L(\mu)]^* H_j^L(\mu) G_F^0, \quad i,j = x_0,y_0,\psi_0 \quad (58)$$

from which the covariance matrix can be obtained

$$\sigma_{ij}^2 = \int_0^{\mu_{max}} G_{ij}(\mu) d\mu$$

Similarly for the radial motion r_o

$$G_{r_or_o}(\mu) = |H_{r_o}^L(\mu)|^2 G_F^0, \quad \sigma_{r_or_o}^2 = \int_0^{\mu_{max}} G_{r_or_o(\mu)d\mu} \quad (59)$$

These quantities are sufficient to completely describe the statistics and probabilities of the linear motions because when the excitation is Gaussian, the motions are Gaussian too.

In order to obtain the PDF's of the mooring system parameters, a joint PDF of the surge, sway, and yaw motions is needed. Utilizing the argument of Gaussianty, it can be written, after [17], as

$$p(x_o,y_o,\psi_o) = p(\mathbf{x} - \bar{\mathbf{x}}) = (2\pi)^{-3/2} |\sigma_{ij}^2|^{-1}$$
$$\times \exp\{-0.5(\mathbf{x} - \bar{\mathbf{x}})^T [\sigma_{ij}^2]^{-1} (\mathbf{x} - \bar{\mathbf{x}})\} \quad (60)$$

where

$|\sigma_{ij}|$ = determinant of the covariance matrix $[\sigma_{ij}^2]$
$(\ )^T$ = transpose matrix
$[\ ]^{-1}$ = inverse matrix
$\mathbf{x} = x_o,y_o,\psi_o$
$\bar{\mathbf{x}} = x_{o_E},y_{o_E},\psi_{o_E}$

The spans of all mooring lines have been shown to be uniquely related to the motions (x_o,y_o,ψ_o). Entering the Catenary Table with these spans, all mooring line parameters can be extracted by interpolation. It follows that the PDF of all parameters is the same as the joint PDF of the motions. For a parameter q this can be written in the form

$$p(q) = p[q(x_o,y_o,\psi_o)] = p(x_o,y_o,\psi_o) \quad (61)$$

It should be remembered, however, that $p(q)$ may no longer be Gaussian, since $q(x_o,y_o,\psi_o)$ is in general strongly nonlinear.

7. Results

The dynamics of a Series 60, $C_B = 0.80$ ship and a disk of diameter-draft ratio 2.5 are examined, both with displacement of 48 117 tonne (t) (47 155 dwt). Both vessels are moored with the same mooring stiffness in water 1000 m (3280 ft) deep with level bottom. The mooring system contains eight identical mooring lines arranged into a spread pattern of 22.5° – 67.5° with port/starboard and fore/aft symmetry. Each line consists of 300-m (984 ft) *ϕ7.62 cm (3 in.) *w21.27-kg/m (14.3 lb./ft) wire (top), 650-m (2132 ft) *ϕ30.5 cm (12.0 in.) neutrally buoyant synthetic rope, and 1250-m (4100 ft) *ϕ7 cm* (2.75 in.) w 97.15-kg/m (65 lb./ft) chain. Figure 8 illustrates partial data of the Catenary Table for these lines. The fairleads on the disk are located at the circumference. Two fairlead arrangements are examined on the ship. In the first, they are located at the bow and stern, in a classical configuration. In the second, a turret configuration is used, where the lines are attached to a ring of 10-m (33 ft) diameter underneath the ship bottom, concentric with the z-axis. The turret is sometimes used to facilitate the ship rotation on station for avoiding the beam-on weather heading.

Four values of the mooring stiffness are examined, expressed in terms of the line pre-tensions equal to 8, 20, 26, and 32 percent of the line breaking strength of 500 tonne.

The weather conditions are varied from a mild Beaufort Force 6, through a severe gale of Force 9 to a violent storm of Force 12. A surface current with a velocity of 2 percent of wind velocity is included. All weather elements are colinear, pointing 165 deg in the global frame.[6]

The foregoing parameters have been selected conservatively; that is, they result in relatively large responses being, perhaps, of limited interest for practical applications but convenient for detecting the nonlinearities.

A short-hand notation is introduced for denoting the vessel-stiffness-weather combinations. The vessels are denoted by D or S for disk or ship; by stiffness, for example, 20% T_{BR}, and by Beaufort Force, for example, BF 12. Example: S – 20%T_{BR} – BF12.

A qualitative examination of the results is presented first on a few selected vessel-stiffness-weather combinations. These re-

[6] Full design particulars of the vessels, moorings, and weather elements and loads are given in reference [1].

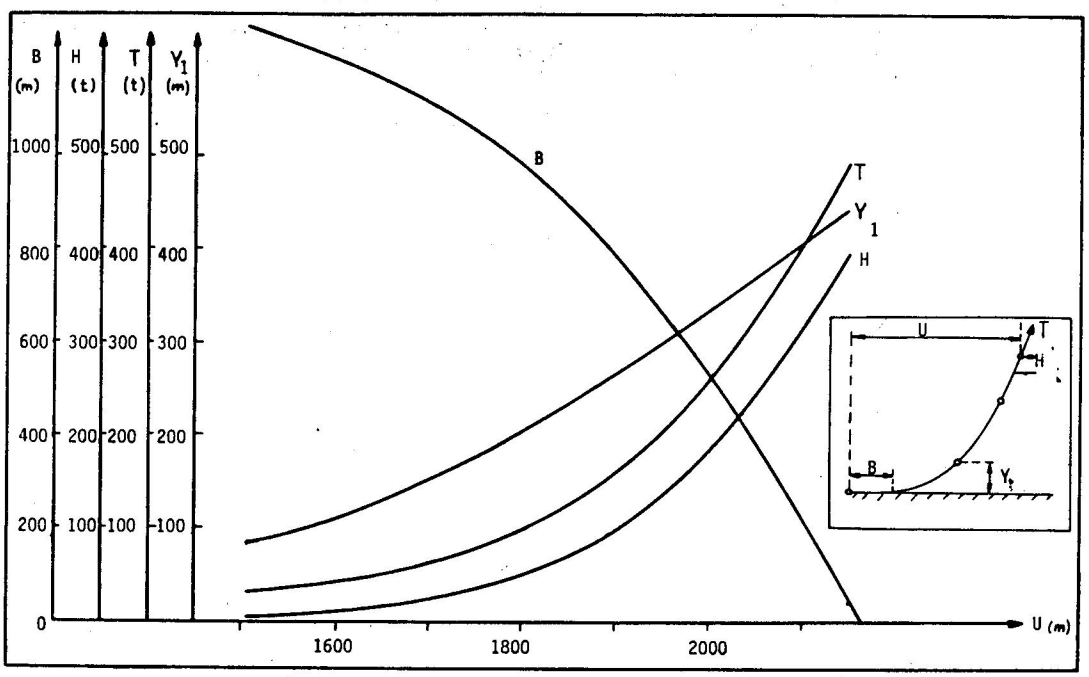

Fig. 8 Partial data of Catenary Table

sults are shown in Figs. 9 through 20; they are summarized in Table 1.

The simulated records shown in Fig. 9 for the "random" case, in Figs. 10–12 for the "regular" case, and in Figs. 18 and 19 for the transient-state case all show the full lengths of the records. Two numbers listed at the grid of each record correspond to the full grid range. The vertical lines in Figs. 10–12 indicate the times of the frequency changes.

The spectra, Figs. 13–15, are shown in four frames. Each frame illustrates the linear and nonlinear excitation spectra by dashed lines and the linear and nonlinear motion spectra by heavy lines, all for one component only. The linear excitation spectra are uniform and the nonlinear excitation spectra are irregular since they are computed from the records. The linear and nonlinear motion spectra are identified by the letters L and N, respectively. The four frames correspond to the following components:

X = spectra of surge, x_o, and of surge excitation, E_{x_o}
Y = spectra of sway, y_o, and of sway excitation, E_{y_o}
ZZ = spectra of yaw, ψ_0, and of yaw excitation, E_{ψ_o}
R = spectra of radius, r_o, and of total exciting force modulus $|E|$

The frequency resolution is shown by a horizontal segment in the upper frame of Fig. 13.

The frequency ranges of the nonlinear excitation spectra can be observed to be somewhat larger than those of the linear ones in the three upper frames of Figs. 13–15. In the lowest frames, the extension is quite significant, and there is a dc level present. The former effect is due to the cosine windows applied to the records prior to the spectral analysis. The latter effect is due to taking the record $|E(t)|$ instead of $E(t)$; that is, it shows the effect of the zero crossings in the total excitation force.

The transfer functions, Fig. 16 and 17, contain four frames, each showing the exact, equivalent-linear (least-square linearized), and linear functions. The four frames correspond, from the top, to the surge, sway, yaw, and radial motions.

The probability density functions, Fig. 20, are shown together with the cumulative probability functions for the excitations and responses.

The different types of nonlinear phenomena are next discussed individually.

Feedback and effect of turret configuration of fairleads. The yaw-excitation feedback can be best observed from the spectra. In the disk case, Fig. 13, where no feedback occurs, the linear and nonlinear excitation spectra are of the same magnitude at all frequencies; they differ only due to the spectral analysis inaccuracies. In the ship case, Fig. 14, there is an evident modulation of the nonlinear excitation at the frequencies where the yaw motion is large. Particularly affected are the sway and yaw excitations. The surge and the total excitations experience a minor modulation. However, the areas under the linear and nonlinear spectra remain of the same order of magnitude for all excitation components. This case represents the ship having the fairleads located at the bow and stern. When the same weather acts on the ship having the fairleads arranged in the turret configuration, Fig. 15, the effect of the feedback becomes profound indeed. The linear and nonlinear excitation spectra now differ by order(s) of magnitude. The turret provides a small yaw-restoring moment; thus the yaw motion is large, with a large dc dynamic level. This causes the weather incidence angle to increase and therefore the weather excitation and motion responses to increase too. When the fairleads are placed at the bow and stern, Fig. 14, the linear theory gives similar results to those of the nonlinear theory, in spite of the violent weather of Force 12. In the turret configuration, Fig. 15, the linear theory clearly ceases to be valid. Figure 12 demonstrates the effect of the feedback in regular records, where the variations of both the magnitude and dynamic mean of the excitation components are evident. In contrast, the excitation on the disk, Fig. 11, remains independent of the yaw motion.

These results indicate that the operational advantage of the fairlead configuration must be carefully traded off in the design with the ship dynamic performance, since too small a turret may easily cause violent ship motions.

Motion coupling. The frequencies of the maximum motions of the disk are practically the same in all motion modes, as can be seen from the spectra, Fig. 13, and from the regular records, Fig. 11. Furthermore, this behavior occurred at all weather and stiffness combinations, although the computed natural frequency of the yaw is between 5 and 12 times the frequency of the surge and sway. This phenomenon is caused by the perfect hydrodynamic disk symmetry, and in the present case the mooring system

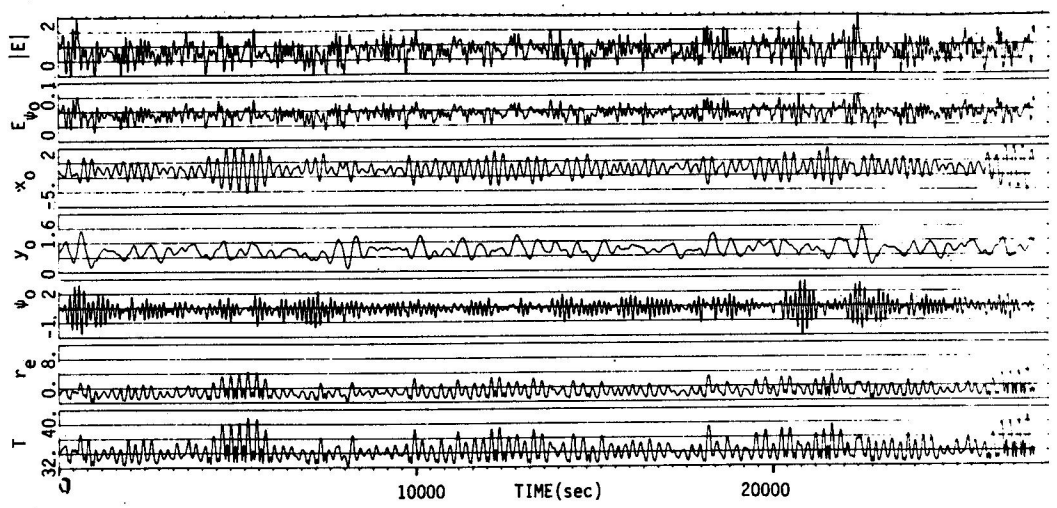

Fig. 9 Random motion records, S-32% T_{BR}—BF6, fairleads at bow and stern

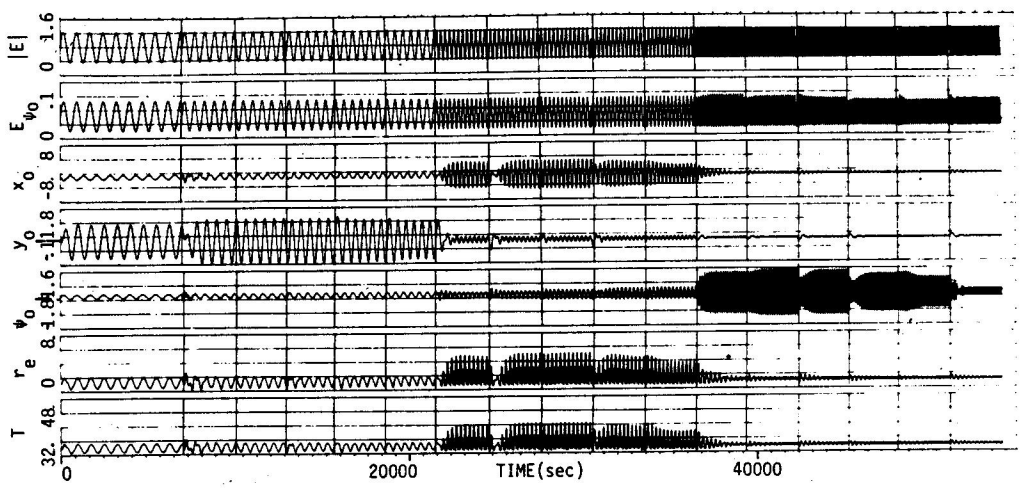

Fig. 10 Regular records, S-32% T_{BR}—BF6, fairleads at bow and stern

Fig. 11 Regular records, D-32% T_{BR}—BF6, fairleads at circumference

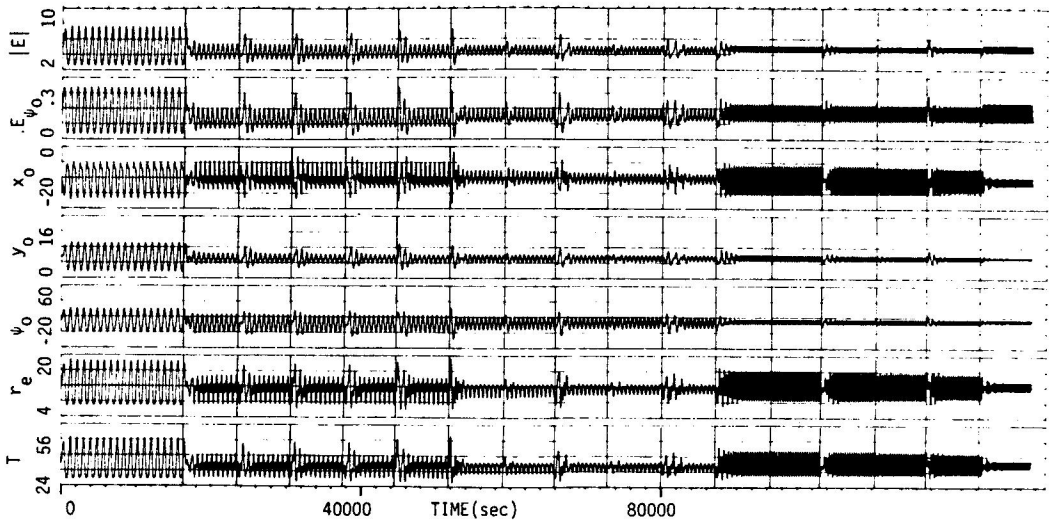

Fig. 12 Regular records, S-20% T_{BR}—BF12, turret configuration of fairleads

is initially symmetric too. The latter symmetry should theoretically vanish under the weather action and it could be expected that the stiffness would be different in the surge and sway modes. The results indicate, however, that the restoring force asymmetry remains sufficiently small to yield practically the same frequencies of resonance in surge and sway. Since the yaw excitation is zero on the disk, the only yaw response is that due to the coupling and it obviously occurs at the frequencies of the surge and sway resonance. In the ship case, the symmetry vanishes and the three resonances are typically quite apart on the frequency axis, Fig. 14. Nevertheless, if the stiffness is sufficiently small, a large weather load may induce such a large motion in one of the modes that the coupling of the restoring forces will override the direct excitation in the other modes and all three modes will then respond at the frequency of the dominant motion. This can be observed in Fig. 17. It is important to note that this behavior can

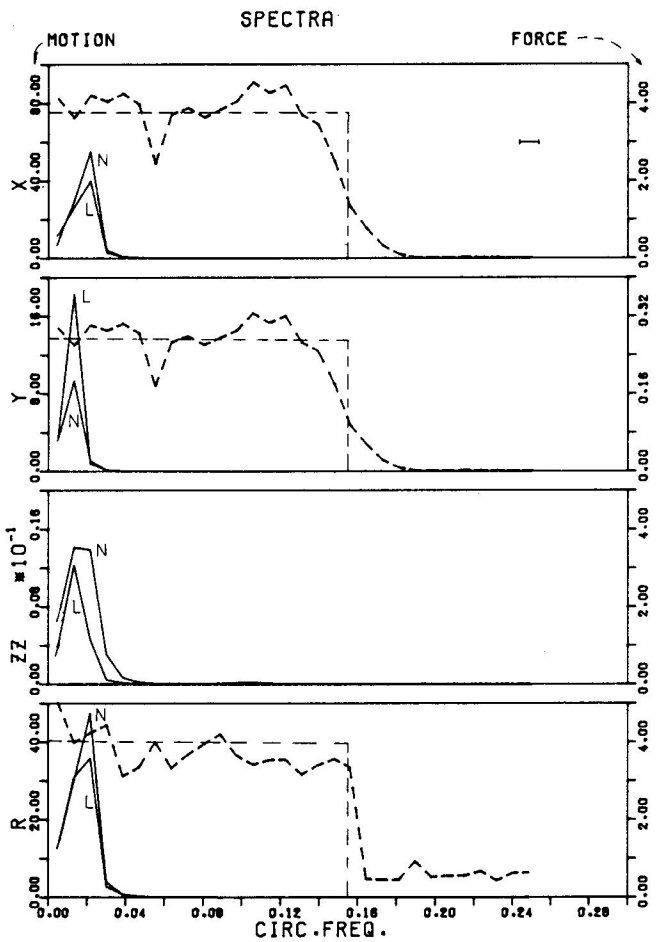

Fig. 13 Spectra, D-32% T_{BR}—BF6, fairleads at circumference

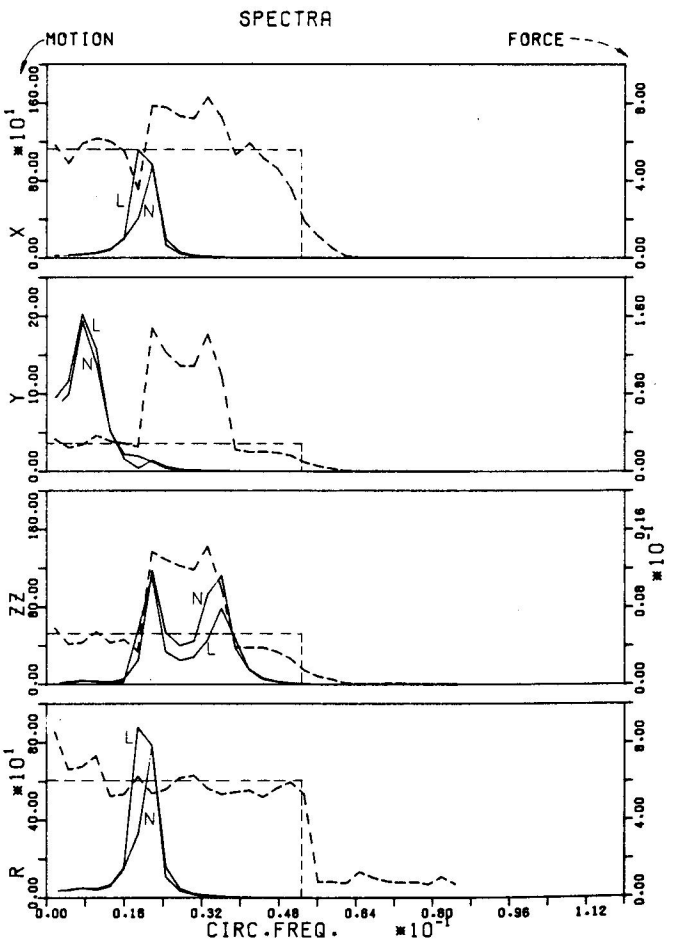

Fig. 14 Spectra, S-20% T_{BR}—BF12, fairleads at bow and stern

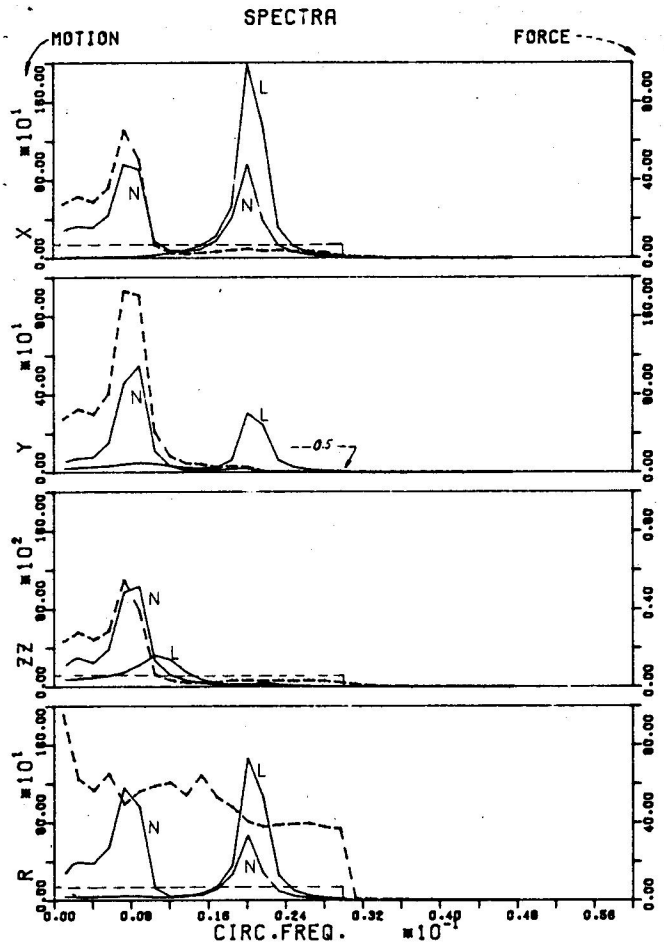

Fig. 15 Spectra, S-20% T_{BR}—BF12, turret configuration of fairleads

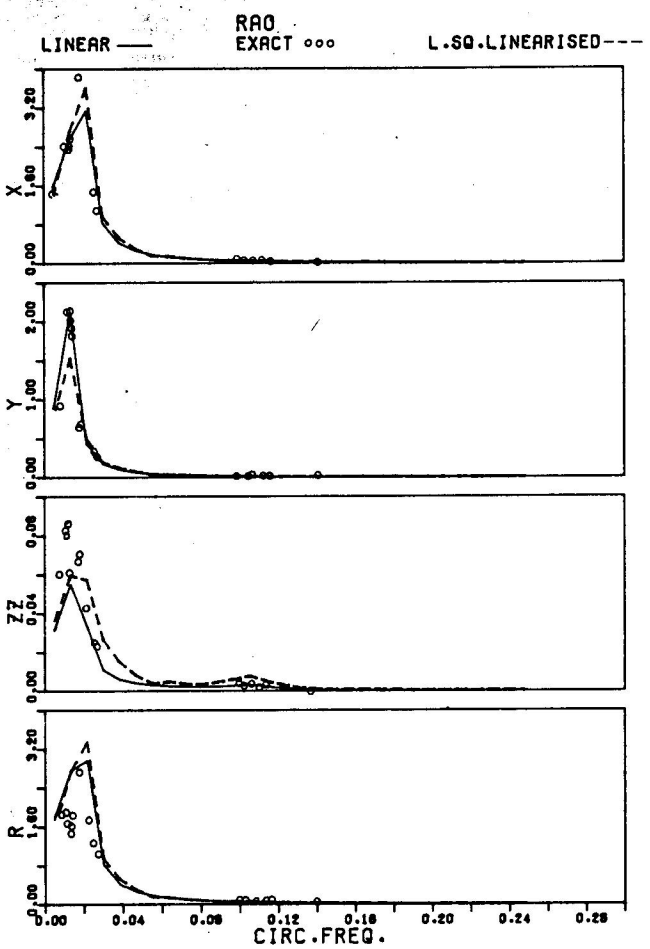

Fig. 16 Motion transfer fuctions, D-32% T_{BR}—BF6, fairleads at circumference

be predicted entirely within the scope of the linear theory.

Superharmonics. The superharmonics occur in the records due to several causes. When the vessel path encloses the origin, the radial motion experiences superharmonics since there occur two radius cycles per one cycle of surge and sway. The same happens to the yaw records since the yaw moment sign then changes four times per motion cycle, as is evident from Fig. 6 (plot of R_{ψ_o}). The superharmonics occur in the tension record whenever x_o, y_o, or ψ_o change sign, since the maximum tension then takes place successively in the leeward, weather, leeward, and weather mooring lines, in each cycle, Fig. 9. The changes of sign of the surge and sway also induce the superharmonics in the radial motion, Fig. 9. The non-linear coupling of the mooring restoring forces may also cause the vessel path to take a zigzag shape. Then, depending on the shape, the superharmonics can occur in any and all motion records. The disk is particularly susceptible to this since it experiences no direct yaw excitation. This type of superharmonics occurred in the yaw, radial, and tension responses of Fig. 11. Typically the superharmonics occur only at high stiffness of the mooring system, that is, when the motions are small. Although the nonlinear superharmonic phenomenon yields interesting vessel behavior, it is of little practical significance in design applications.

Jump and frequency shift. A well-established fact in the theory of nonlinear vibrations is that a nonlinear spring may cause the jump phenomenon. When the spring is hard, the peak of the transfer function folds over toward higher frequencies. Provided the peak is sufficiently prominent and the shift large enough, the function becomes triple-valued, thus causing the response to jump from the highest to the lowest branch with increasing excitation frequency and the opposite with decreasing frequency. When the spring is soft, the peak folds over toward lower frequencies and the situation is reversed. Of the three transfer functions examined here—linear, equivalent-linear and exact—it is only the latter that can show this behavior through a histerisis loop, if any. The equivalent-linear function may indicate only a frequency shift of the peak.

No jump has been observed in any of the cases examined here. The shapes of the functions vary from these, corresponding to the most-linear motions in Fig. 16 (lowest weather load and highest stiffness), to those, corresponding to the most-nonlinear motions in Fig. 17 (highest weather load and lowest stiffness). The lack of jump can be attributed to any and all of the following interacting phenomena. Firstly, the nonlinearity of the mooring forces may not be sufficiently large to cause the jump. Secondly, the coupling of the three spring components may redistribute the potential energy of the springs. That is, when the system is deflected primarily against one of the springs and this spring becomes saturated with potential energy, the remaining springs may take over the deflections before the first spring is sufficiently deflected to yield the jump. This would also explain the zigzag path of the vessel, observed in several cases. Thirdly, the exact transfer functions have the peaks lower than the remaining two functions since the energy of their harmonic excitation is concentrated at a single frequency; thus it overemphasizes the nonlinearity at that frequency and therefore reduces the response. (A spectrum of the harmonic excitation is a Dirac function while in the random case it is finite, spread over a finite frequency range.) A lower peak obviously delays the jump phenomenon. The lower peaks can be clearly seen in Fig. 17.

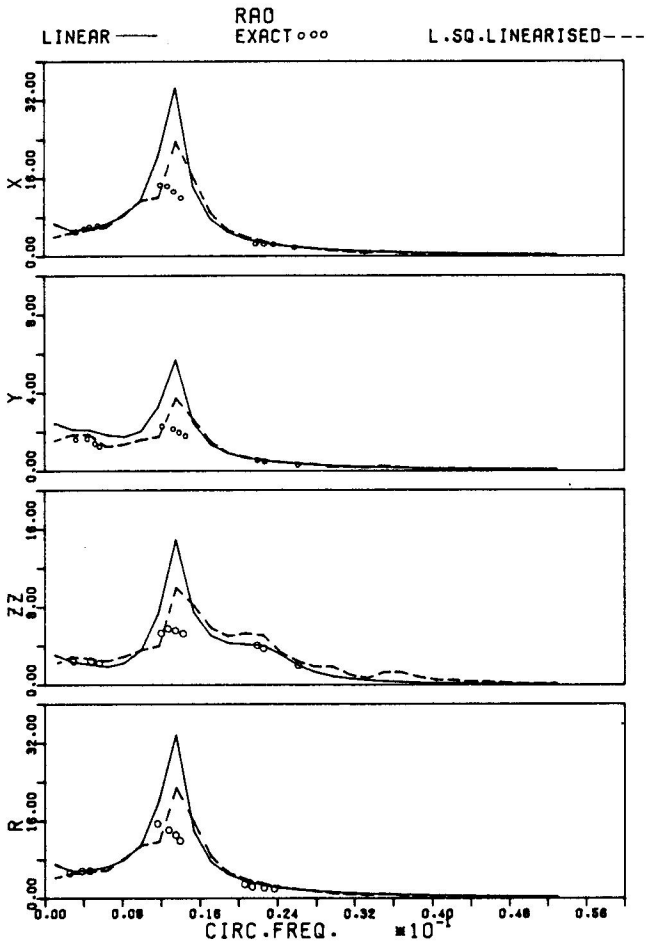

Fig. 17 Motion transfer functions, S-8% T_{BR}—BF12, fairleads at bow and stern

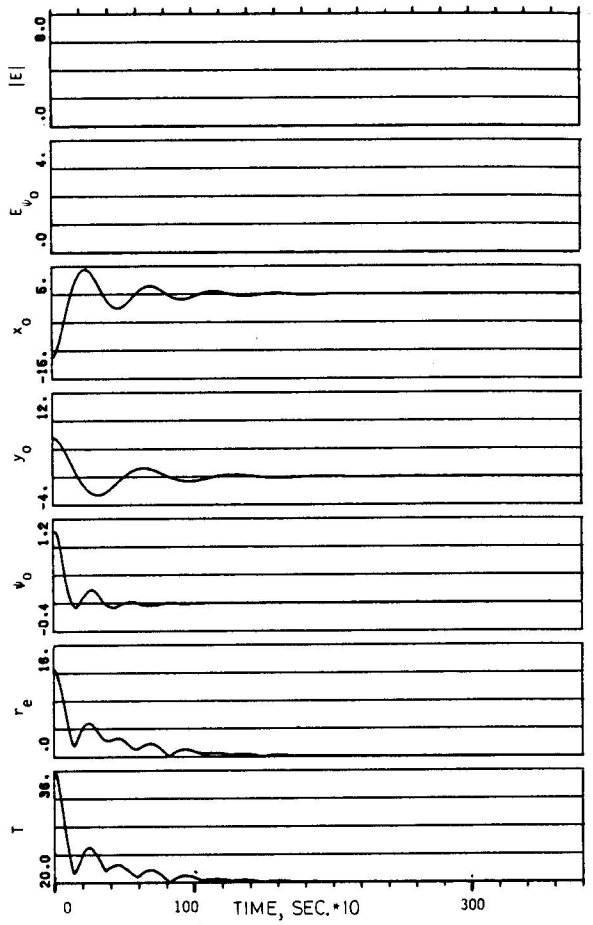

Fig. 18 Transient-state simulation with linear and nonlinear damping, D-20% T_{BR}—BF12

Although the occurrence of the jump cannot be entirely ruled out in the multileg mooring applications, the foregoing results indicate that the likelihood of it is small.

Harmonicity and periodicity. The nonlinearity of the damping forces combined with the large excitation may cause a nonharmonic or even a nonperiodic response to a harmonic excitation. These so-called relaxation oscillations occurred in the case of the lowest stiffness and highest weather load on the ship with the turret, Fig. 12. The responses of surge (and consequently of radius and tension) show a strong nonharmonic behavior although it is still periodic.

Cubic damping in transient states. Figures 18 and 19 illustrate the transient-state records simulated, respectively, with and without the cubic-damping terms in the equations of motion. The motion extinction tests such as these can be realized experimentally for calibrating the cubic damping. It is important, however, that the actual tests be performed in the presence of the waves, so that the turbulence induced by the high-frequency motions can be properly simulated. The measured motions must then obviously be filtered out before the comparisons with the low-frequency simulation can be made.

Probabilities. Figure 20 illustrates a typical set of the measured probability functions. Table 2 presents the results of the χ-square tests applied to the excitation and response probabilities to check whether they are normally distributed. The tested conditions include the extreme vessel-stiffness-weather combinations.

The results for the turret case indicate that the assumption of Gaussianity is unacceptable. In the bow-stern fairlead configuration, the surge and to a slightly lesser degree the sway appear to be normal in all cases. The yaw remains Gaussian when the motions are large but ceases to be Gaussian when the motions are small, due to the presence of superharmonics. However, since the superharmonics occur only when the motions are small, the effect of the non-Gaussian distribution of the yaw can be neglected in practical applications and all three primary motions can be assumed to be Gaussian. This assumption is important since in order to utilize the linear theory for predicting the mooring system probabilities, the surge, sway, and yaw motions must all be assumed to be Gaussian.

It is interesting to note from Table 2 that the excitation components have a small probability of being Gaussian, in spite of the fact that the signal $Q(t)$ in the excitation is Gaussian by definition. In the case of E_{ψ_o} this is caused by the feedback from the non-Gaussian yaw motion and in the case of the excitation force it is the result of both the feedback and the modulus of the excitation force $|E|$.

Natural frequencies. The natural frequencies of the surge, sway, and yaw motions are plotted in Fig. 21 for all vessel-stiffness-weather combinations. The influence of the weather strength becomes negligible when the initial system stiffness is large. The highest frequency of all cases is 0.11 rad/s. This value is well below the wave frequency range (typically, 0.2 to 2 rad/s); therefore the separation of the low- and high-frequency regions is fully justified.

Mooring-system parameters. Figure 22 illustrates the mean and rms values of the maximum tension record computed from the simulations. The mean tension increases monitonically with the initial stiffness and with the weather load, as expected. The variation of the tension rms with pretension is nonmonotonic;

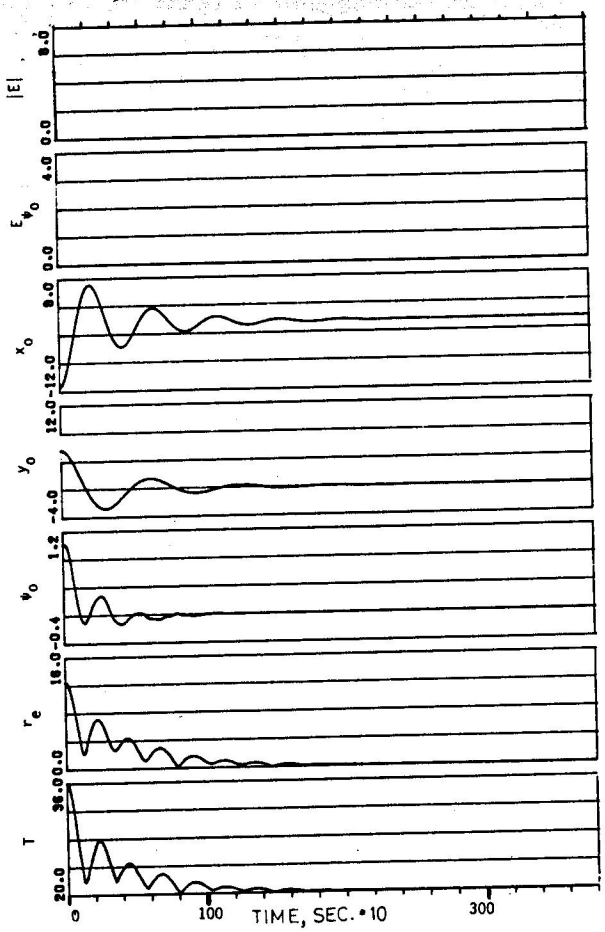

Fig. 19 Transient-state simulation with linear damping only, *D*-20% T_{BR}—BF12

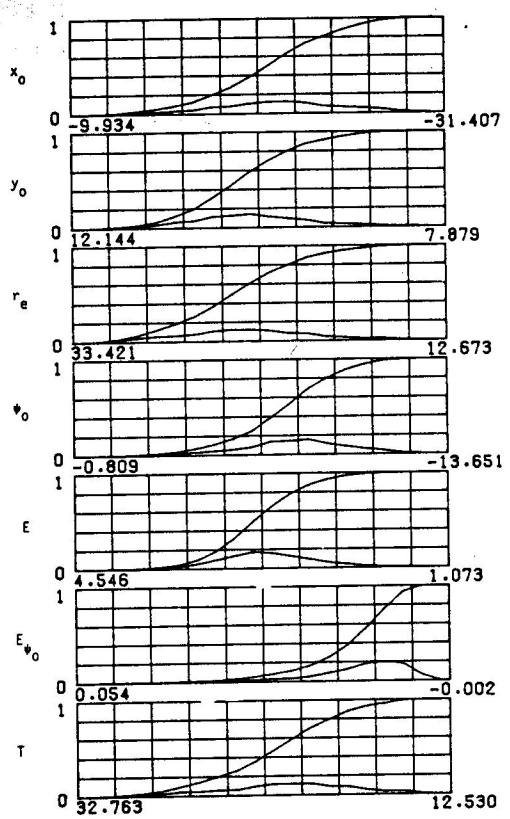

Fig. 20 Probability density and cumulative functions, S-8% T_{BR}—BF12

there exist a pre-tension yielding the minimum oscillatory tension. This behavior may suggest an optimization of the mooring-system stiffness; however, it would not be practical since the oscillatory tension is only a small fraction of the mean tension and the latter increases monotonically with the pre-tension. Therefore the total tension has no minimum in the dynamic sense, and from the structural point of view the pre-tensions should be kept as low as possible. The remaining mooring parameters are related to the tension values through the Catenary Table, which is partly illustrated in Fig. 8.

The remaining discussion contains comparisons between the linear and nonlinear theory results for all vessel-stiffness-weather combinations examined.

Linear versus nonlinear excitation. Figures 23 and 24 present the comparison of the linear and nonlinear values of the excitation components. The linear and nonlinear results are presented by continuous and dashed lines, respectively, or, where the two overlap, by a line which is partly dashed and partly continuous. The agreement between the two theories is remarkable in most conditions. In the disk case both theories should give the same results by definition, due to disk symmetry. The differences would be attributable only to the finite accuracy of the spectral analysis, but they can be seen to be negligible.

There is a dc level induced by the feedback on the sway and yaw mean values at the least realistic combination of the lowest stiffness and highest weather. Even then, the difference is only

Table 1 Summary of graphical output quoted

Fig. No.	Vessel-Stiffness-Weather	Fairleads Configuration	Contents
9	S-32%T_{BR}—BF6	bow and stern	random records
10	S-32%T_{BR}—BF6	bow and stern	regular records
11	D-32%T_{BR}—BF6	circumference	regular records
12	S-20%T_{BR}—BF12	turret	regular records
13	D-32%T_{BR}—BF6	circumference	spectra
14	S-20%T_{BR}—BF12	bow and stern	spectra
15	S-20%T_{BR}—BF12	turret	spectra
16	D-32%T_{BR}—BF6	circumference	motion transfer functions
17	S-8%T_{Br}—BF12	bow and stern	motion transfer functions
18	D-20%T_{BR}—BF12	circumference	transient simulation with linear and nonlinear damping
19	D-20%T_{BR}—BF12	circumference	transient simulation with linear damping only
20	S-8%T_{BR}—BF12	bow and stern	probability functions

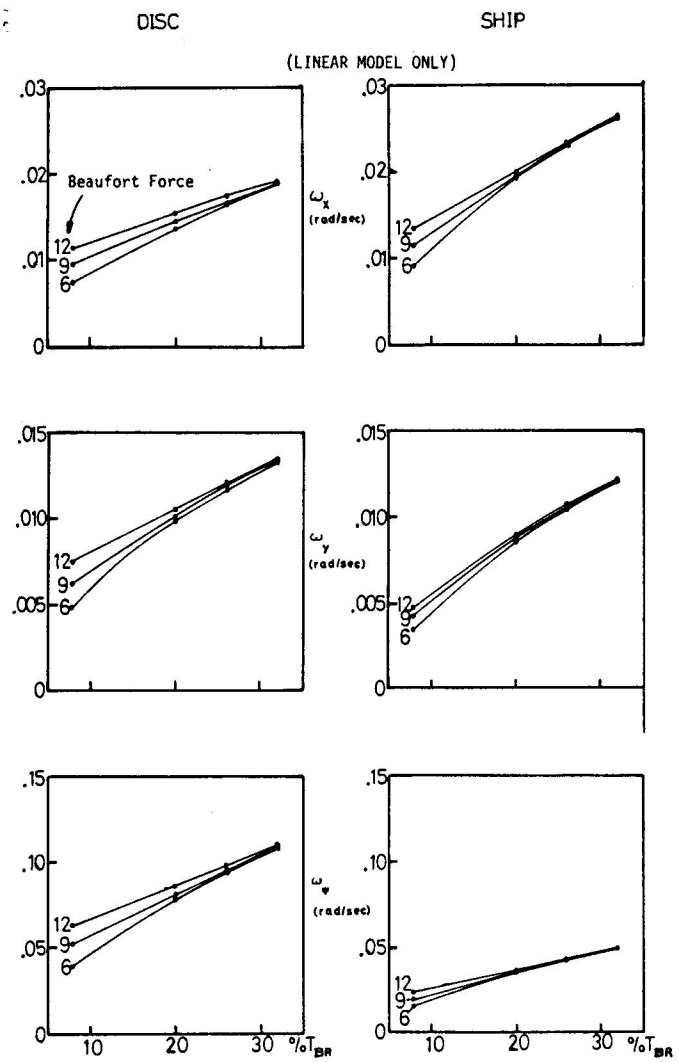

Fig. 21 Natural frequencies

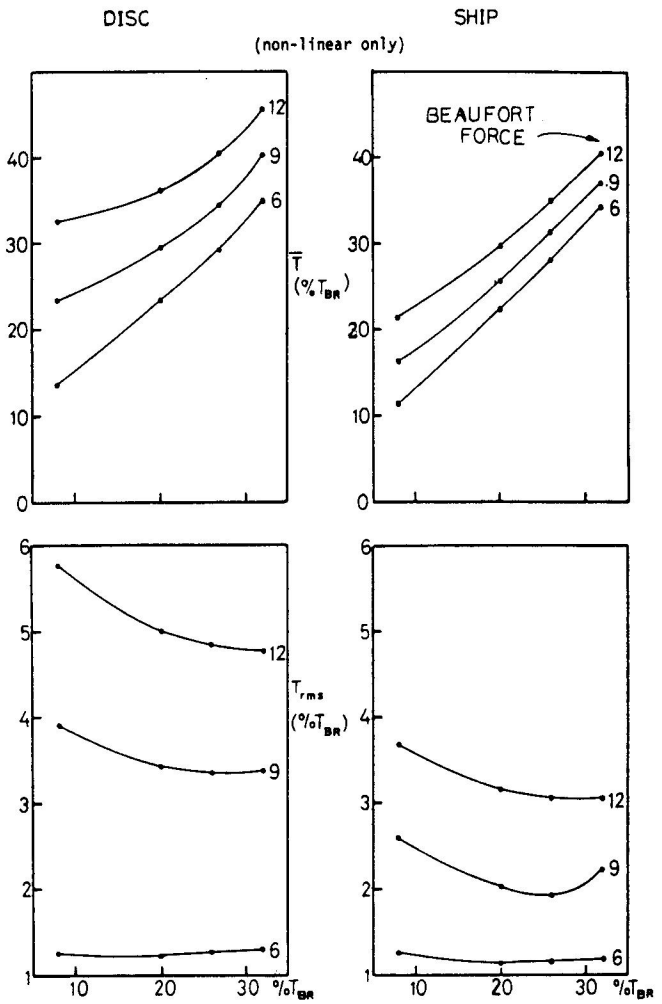

Fig. 22 Mean and rms values of mooring line tensions

12 percent. At higher stiffnesses, both theories agree to within 3 percent, even for the violent-storm condition.

The differences between the linear and nonlinear excitations on the ship are more pronounced, caused again by the feedback. However, disregarding the unrealistic low-stiffness cases, the differences are less than 13 percent, and at the highest stiffness they become negligible again.

Linear versus nonlinear motion responses. Figures 25 and 26 present the mean and rms motion responses. The mean values of all responses are predicted almost identically by the linear and nonlinear theories, thus indicating that the dynamic dc levels are negligible. The oscillatory motion predictions differ significantly between the theories when the stiffness is low, but at the more realistic stiffness values the agreement is within 15 percent. In general, the agreement is better for the disk than for the ship, as expected, since the disk dynamics are subject to fewer nonlinearities.

The oscillatory responses decrease with increasing stiffness at a much slower rate than the mean responses. Thus the dynamic contributions play an increasing role with both increasing stiffness and increasing weather. Even at the lowest stiffness, however, the dynamic effects cannot be neglected, the rms motions being then equal to between 7 and 67 percent of the mean motions. It follows that the static mooring model is rather inadequate on its own.

8. Conclusions

Three theories of the moored ship and disk performance have been demonstrated, linear and nonlinear dynamic for the low-

Table 2 Probability of variables being Gaussian

Vessel	Fairleads	Stiffness, %T_{BR}	Weather, BF	p(Variable Is Normally Distributed) x_o	y_o	ψ_o	r_e	$\lvert E\rvert$	E_{ψ_o}	T
Ship	bow/stern	8	12	0.9998	0.9083	0.9922	0.9999	0.0117	0	0.9997
	bow/stern	32	6	0.9839	0.9562	0.0076	0.8521	0.7589	0.9736	0
Disk	circumference	8	12	0.9999	0.9816	0.7285	0.9998	0.9812	...	0
	circumference	32	6	0.9547	0.9118	0	0.8127	0.6926	...	0.9530
Ship	turret	20	12	0.0001	0.9973	0	0	0.9654	0.6006	0.0002

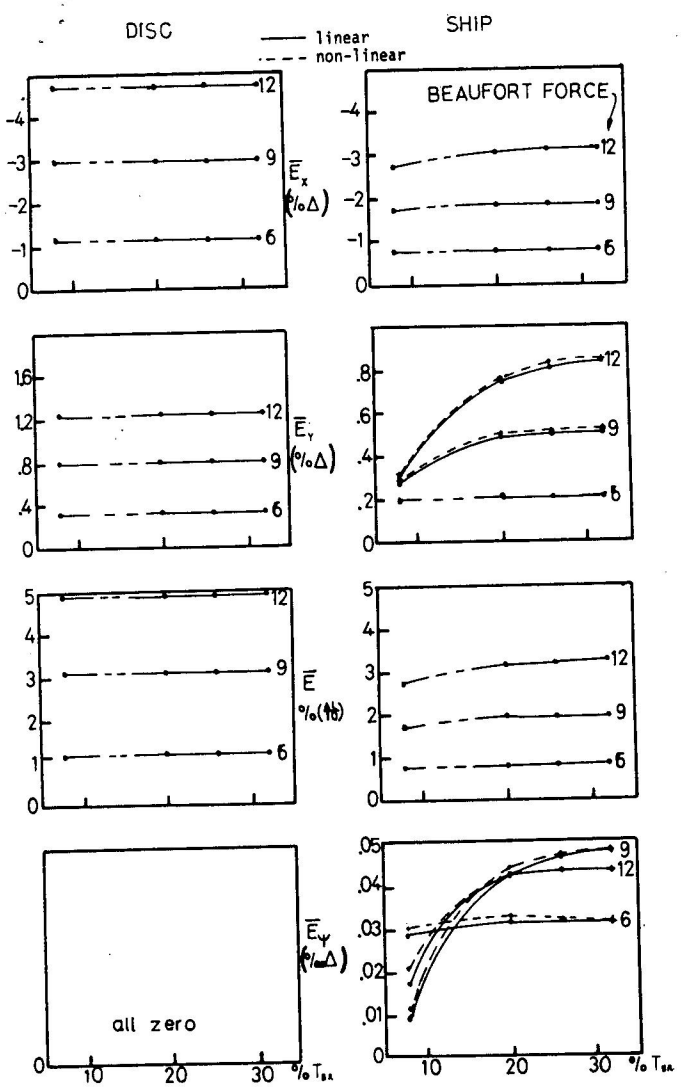

Fig. 23 Mean excitation components

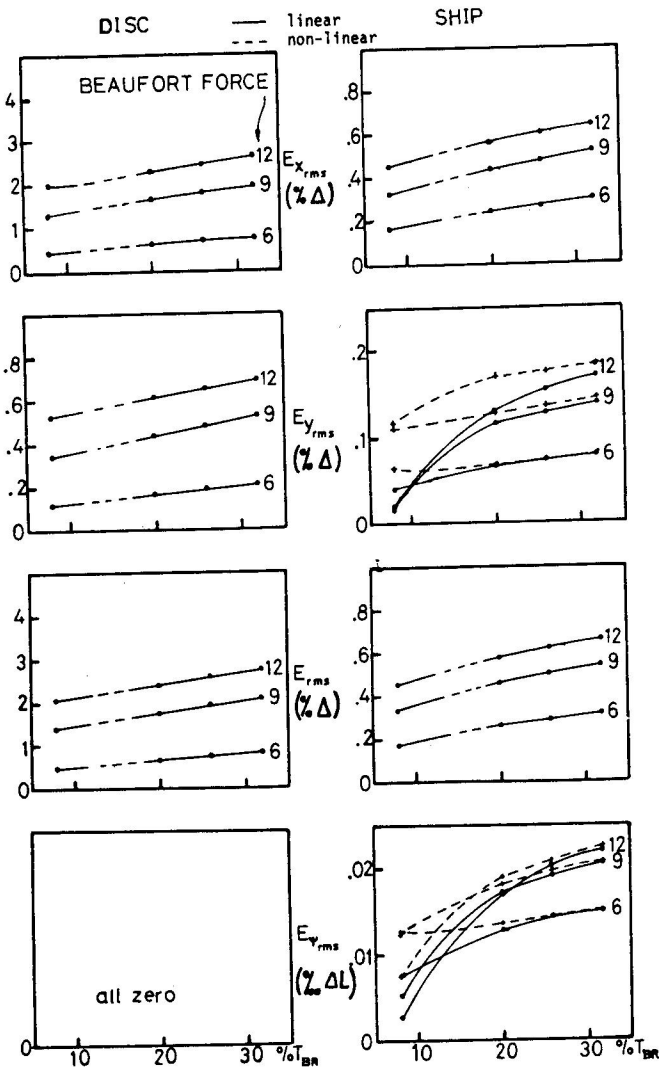

Fig. 24 Rms values of excitation components

frequency problem, and a static model which represents the mean values (and is a by-product) of the linear theory. The static model is inadequate on its own; the dynamic contributions are between 7 and 67 percent of the static values in the examples examined here. The linear dynamic theory is adequate in the limited class of applications where the vessel motions are small and where the fairleads are located sufficiently far from the vessel center of gravity. The present standards of the offshore oil industry limit the maximum horizontal vessel motion to 4 to 8 percent of water depth. In this range the linear theory can be used with confidence. The nonlinear phenomena that occur then are not important quantitatively and the linear predictions are within 10 to 15 percent of the nonlinear ones. For the analysis of larger motions, the nonlinear theory should be used. Also, the analysis of a ship having a turret configuration of the fairleads should always be based on the nonlinear theory, since such a configuration may cause quite violent vessel motions.

Both theories are totally automated. The computing time for one vessel-stiffness-weather case using the linear theory is 50 s on the ICL2970 and 3 s on the CDC7600 machines. The nonlinear theory, including the spectral analysis and plotting, takes 600 to 900 s and 25 to 40 s, respectively, on the two computers.

References

1 Oppenheim, B. W., "Low-Frequency Dynamics of Moored Vessels," Ph.D. Thesis, Ship Science, University of Southampton, Southampton, England, Jan. 1980.

2 Johansson, P. I., "A Finite Element Model for Dynamic Analysis of Mooring Cables," Ph.D. Thesis, Massachusetts Institute of Technology, Cambridge, Mass., 1976.

3. Oppenheim, B. W. and Wilson, P. A., "Polynomial Representation of Coupled Mooring Forces," *Journal of Ship Research*, to be published.

4 Faltinsen, D. and Michelsen, F. C., "Motions of Large Structures in Waves of Zero Froude Number," *Proceedings*, International Symposium on the Dynamics of Marine Vehicles and Structures in Waves, London, 1974.

5 Abkowitz, M. A., *Stability and Motion Control of Ocean Vehicles*, MIT Press, Cambridge, Mass., 1970.

6 Shampine, L. F. and Gordon, M. K., *Computer Solutions of Ordinary Differential Equations*, W. H. Freeman & Co., San Francisco, 1975.

7 Newman, J. N., "Second-Order, Slowly Varying Forces on Vessels in Irregular Waves," *Proceedings*, International Symposium on the Dynamics of Marine Vehicles and Structures in Waves, London, 1974.

8 Faltinsen, O. M. and Løken, A., "Slow Drift Oscillations of a Ship in Irregular Waves," Det norske Veritas, No. 108, 1979 (also the preprint with additional figures).

9 "Recommended Practice for Mooring Offshore Floating Vessels," American Petroleum Institute, 1974 (proposal).

10 Remery, G. F. M. and Herman, A. J., "The Slow Drift Oscillations of a Moored Object in Random Waves," Offshore Technology Conference, OTC-1500, Houston, Texas, 1971.

11 Newman, J. N., "The Drift Force and Moment on Ships in Waves," *Journal of Ship Research*, Vol. 11, No. 1, March 1967.

12 Salvesen, N., "Added Resistance of Ships in Waves," *Journal of Hydronautics*, Vol. 12, No. 1, 1978.

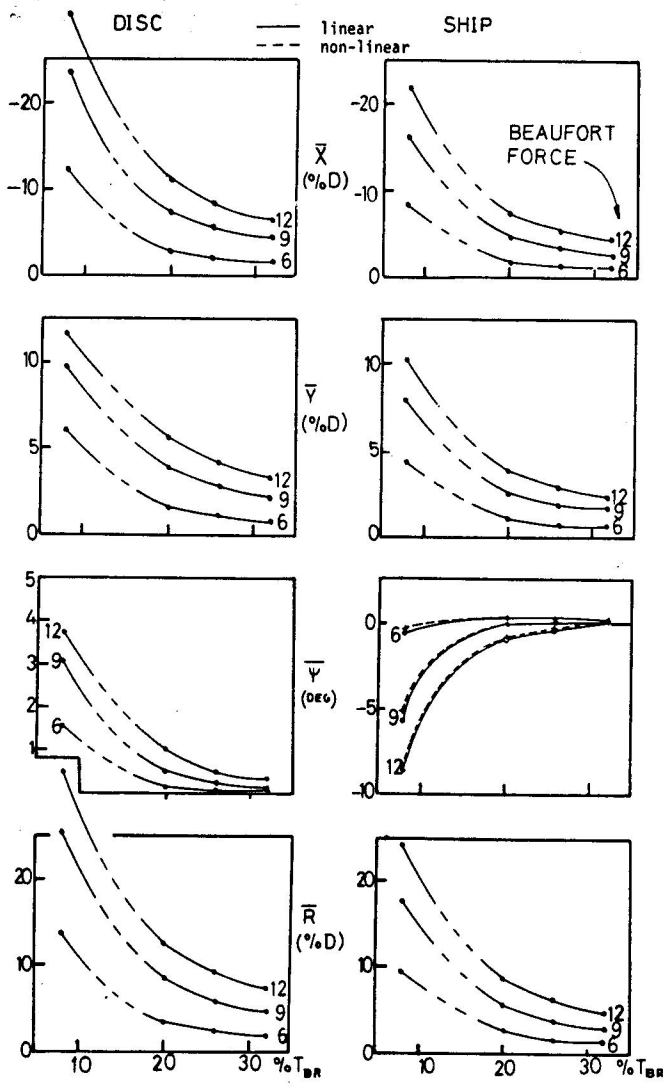

Fig. 25 Mean motion response components

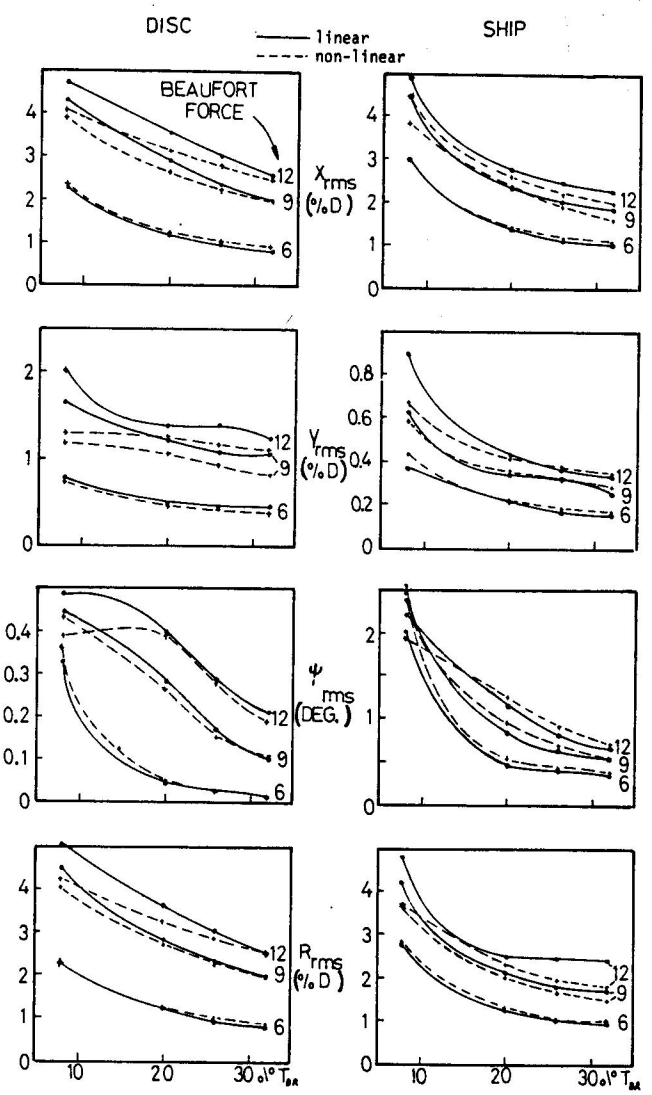

Fig. 26 Rms values of motion response components

13 Hsu, F. H., "Analysis of Peak Mooring Forces Caused by Slow Vessel Drift Oscillations in Random Seas," Offshore Technology Conference, OTC-1159, Houston, Texas, 1970.

14 Pinkster, J. A., "Low-Frequency Phenomena Associated with Vessels Moored at Sea," *Society of Petroleum Engineers Journal*, SPE-4837, 1974.

15 Newland, D. E., *An Introduction to Random Vibrations and Spectral Analysis*, Longman, London, 1975.

16 Oppenheim, B. W. and Wilson, P. A., "Continuous Digital Simulation of the Second-Order Slowly-Varying Wave Drift Force," *Journal of Ship Research*, Vol. 24, No. 3, Sept. 1980.

17 Lin, Y. K., *Probability Theory of Structural Dynamics*, McGraw-Hill, New York, 1977.

18 Abkowitz, M. A., "Lectures in Ship Hydrodynamics, Steering and Manueverability," Hydro-Og, Aerodynamisk Laboratory Report Hy-5, Lyngby, May 1964.

19 Price, W. G. and Bishop, R. E. D., Denmark, *Probabilistic Theory of Ship Dynamics*, Chapman and Hall, London, 1974.

20 von Kerczek, C. and Tuck, E. O., "The Representation of Ship Hulls by Conformal Mapping Functions," *Journal of Ship Research*, Vol. 13, No. 4, Dec. 1969.

21 Salvesen, N., "Ship Motions and Sea Loads," *Trans.* SNAME, Vol. 78, 1970.

22 Oppenheim, B. W. and Wilson, P. A., "Static 2-D Solution of a Mooring Line of Arbitrary Composition in the Horizontal and Vertical Operating Modes," *International Shipbuilding Progress*, to be published.

23 Strom-Tejsen, J. and Chislet, M. S., "A Model Testing Technique and Method of Analysis for the Prediction of Steering and Maneuvering Qualities of Surface Vessels," Report No. Hy-7, Hydro-Og Aerodynamics Laboratory Lyngby, Denmark, 1966.

Appendix

Expansion of external forces

The forces X, Y, and N in equation (5) represent the total body forces dependent on the position, velocity and acceleration vectors, as well as the excitation forces dependent on these vectors and on the weather elements and time. Assigning the force signs so that the positive excitation forces oppose the positive body forces, this dependence is written in the form

$$X_i = E_i\,(\text{weather}, t, x, y, \psi, \dot{x}, \dot{y}, \dot{\psi}, \ddot{x}, \ddot{y}, \ddot{\psi}) - X_i'(x, y, \psi, \dot{x}, \dot{y}, \dot{\psi}, \ddot{x}, \ddot{y}, \ddot{\psi})$$

where

$$E_i = E_x, E_y, E_\psi = \text{excitation forces}$$
$$X_i' = X, Y, N = \text{body forces}$$

The dependence of the excitation on the velocities and accelerations can be immediately disregarded upon noticing that the low-frequency velocities and accelerations are orders of magnitude smaller than those of the weather elements (typical vessel velocity is of the order of a small fraction of m/s). The dependence of the excitation forces on the vessel position is further disposed of using the argument that the wave forces correct to the sec-

ond-order depend only on the first-order motions and wave excitation, and the effect of the position-dependent mooring forces on the first-order quantities is negligible due to the relatively large vessel mass. The effect of the vessel angular orientation, ψ, is, however, included, since in view of the large and slow yaw allowed here, the incidence angle of the weather elements can strongly vary and this may introduce large changes of the wind, current, and wave forces. Thus the excitation forces take the form $E_i = E_i$ (weather, t, ψ) and they are written in a short-hand form as $E_i = E_i(t)$.

The body forces are expanded into a Taylor series

$$X'_i = X'_{i_x}x + X'_{i_y}y + X'_{i_\psi}\psi + \ldots + X'_{i_{\dot\psi}}\ddot\psi + \frac{1}{2!}[X'_{i_{xx}}x^2 + \ldots + X'_{i_{\psi\psi}}\psi^2 + X'_{i_{xy}}xy + \ldots + X'_{i_{\dot y\dot\psi}}\ddot y\ddot\psi + \frac{1}{3!}[\ldots\ldots] + \ldots\ldots$$

where the subscripts denote the partial derivatives of X' with respect to x,y,ψ and their derivatives. The terms are next grouped by collecting the acceleration terms under a common name A, velocity (damping) terms under D, position (restoring) terms under R, and the coupling cross-terms under AD, AR, DR and ADR, respectively.

$$\begin{aligned} X'_i = {} & A_i(\ddot x,\ddot y,\ddot\psi,\ddot x^2,\ddot y^2,\ddot\psi^2,\ddot x\ddot y, \quad \ldots) \\ & + D_i(\dot x,\dot y,\dot\psi,\dot x^2,\dot y^2,\dot\psi^2,\dot x\dot y, \quad \ldots) \\ & + R_i(x,y,\psi,x^2,y^2,\psi^2,xy, \quad \ldots) \\ & + AD_i(\ddot x\dot x,\ddot x\dot y,\ddot x\dot\psi,\ddot y\dot y,\ddot y\dot\psi,\ddot\psi\dot\psi, \quad \ldots) \\ & + AR_i(\ddot x x,\ddot x y,\ddot x\psi,\ddot y y,\ddot y\psi,\ddot\psi\psi, \quad \ldots) \\ & + DR_i(\dot x x,\dot x y,\dot x\psi,\dot y y,\dot y\psi,\dot\psi\psi, \quad \ldots) \\ & + ADR_i(\ddot x\dot x x,\ddot y\dot y y,\ddot\psi\dot\psi\psi,\ddot x\dot x y, \quad \ldots) \end{aligned}$$

The terms AD and ADR are neglected following [18], where it is stated that there is no significant interaction between the viscosity and inertia properties of the fluid and also that the acceleration forces calculated from the classical potential theory give the linear terms only. Thus the acceleration terms A_i take the simple form

$$A_i = a_{i1}\ddot x + a_{i2}\ddot y + a_{i3}\ddot\psi, \quad i = x,y,\psi \tag{62}$$

Although only the linear terms are present in (62), they represent the second-order terms since the low-frequency accelerations are of second order. The mass of the mooring system can be shown to be negligible relative to the vessel mass.

The damping forces consist of the wave damping and viscous damping. The former is disregarded in view of the slow motion considered here. The viscous damping due to the vessel (that is, disregarding the mooring-line damping), expanded up to the second order, is

$$D_i = b_{i1}\dot x + b_{i2}\dot y + b_{i3}\dot\psi + c_{i1}\dot x^2 + c_{i2}\dot y^2 + c_{i3}\dot\psi^2 + c_{i4}\dot y\dot\psi + c_{i5}\dot x\dot y + c_{i6}\dot x\dot\psi$$

To the authors' knowledge, there are no data on the low-frequency damping in the presence of the high-frequency motion components. The closest information available is that for ships maneuvering in calm water at nonzero Froude number [18,23]. It is demonstrated therein that the terms $\dot x\dot y$ and $\dot x\dot\psi$ are zero in the longitudinal force D_x, and are small in the forces D_y and D_ψ on vessels with port/starboard (P/S) symmetry. The only cross-term which is not zero is $\dot y\dot\psi$. The terms $\dot x^2$, $\dot y^2$ and $\dot\psi^2$ are inconvenient to use because of the signs; instead, two other forms are used in the literature, either $\dot x|\dot x|$, $\dot y|\dot y|$ and $\dot\psi|\dot\psi|$, or $\dot x^3$,$\dot y^3$ and $\dot\psi^3$. In the present work the latter form is favored. The total expansion thus takes the form

$$D_i = b_{i1}\dot x + b_{i2}\dot y + b_{i3}\dot\psi + c_{i1}\dot x^3 + c_{i2}\dot y^3 + c_{i3}\dot\psi^3 + c_{i4}\dot y\dot\psi \tag{63}$$

Using this general notation, it is necessary to point out that the following terms are always zero due to the P/S symmetry on ships[7]:

$$b_{12} = b_{21} = b_{13} = b_{31} = c_{12} = c_{21} = c_{13} = c_{31} = 0$$

In the disk case, due to the circular symmetry, the following additional coefficients also vanish

$$b_{23} = b_{32} = c_{23} = c_{32} = 0$$

The foregoing expansion is due to the vessel only. The additional damping due to the mooring lines is assumed to be linear only.

The mooring restoring forces R are evaluated numerically in Section 4.

The velocity and acceleration vectors are independent of the position vector; hence the groups AR and DR due to the vessel are both zero. On the other hand, these groups are not zero due to the mooring lines since both the accelerations and damping of a line element depend on its stiffness, that is, indirectly on the line geometry, and this changes with the vessel position vector (x,y,ψ). In order to compute these terms, however, it would be necessary to evaluate the line geometry by a finite-element method and to keep track of the position and quasi-static velocity and acceleration of each element in each line in the mooring system at all times during the simulation. The computational realism precludes this approach at present; therefore the groups AR and DR are disregarded altogether. It is likely that these groups may be small indeed. The damping on the mooring lines is important only on the slack lines, and those contribute less to the system dynamics than the taut lines. Thus the group DR may be quite small. Similarly, since the group A is negligible on the mooring lines, the group AR can be expected to be small too.

In summary, it can be stated that the linear theory of the moored-vessel dynamics contains a full expansion of the forces up to the second order, and the nonlinear theory contains a partial expansion of the third-order.

Hydrodynamic coefficients

The added mass in the horizontal motion can be shown from the free-surface boundary condition to approach a constant value at low frequency. The constant value is equal to the added mass of a double body in unbounded fluid. Utilizing this fact, the added mass matrix $[a_{ij}]$ is estimated for the ship using the strip theory [19], where the sectional mass is computed from the Lewis Section theory [20]. This yields a_{22}, $a_{23} = a_{32}$ and a_{33}. The ship surge mass, a_{11}, is approximated by that of an ellipsoid moving along its longest axis. The remaining terms $(a_{12},a_{21},a_{13},a_{31})$ are all zero because of the P/S symmetry [19]. The added mass of a disk is equal to the displaced mass, $a_{11} = a_{22} = m$, and the remaining terms are all zero in view of the circular disk symmetry.

The linear and cubic damping matrices $[b_{ij}]$ and $[c_{ij}]$ have been estimated from the tabulated data on the quadratic drag in steady flow [9].

[7] Because of the lack of reliable data, the coefficient of the term $\dot y\dot\psi$ has been assumed to be zero in the calculations quoted in Section 7. This assumption is valid for the disk but not for the ship. However, this assumption has made the results more conservative; namely, the nonlinear motions are overestimated, together with the other nonlinearities. Therefore, all qualitative conclusions and comparisons still remain valid on the conservative side.